NASA CR 159847

TWO-PHASE WORKING FLUIDS FOR THE TEMPERATURE RANGE 50-350°C (PHASE II)

Prepared Under Contract No. NAS3-21202

by
Sigma Research, Inc.
2950 George Washington Way
Richland, Washington 99352
for
LEWIS RESEARCH CENTER
National Aeronautics and Space Administration
Cleveland, Ohio

SIGMA RESEARCH, INC.
2950 GEORGE WASHINGTON WAY
RICHLAND, WASHINGTON 99352
(509) 375-0663

1. Report No.	2. Government Accession No.	3. Recipient's Catalog No.
NASA CR-159847	--	--

4. Title and Subtitle	5. Report Date
Two-Phase Working Fluids for the Temperature Range 50 to 350°C Phase II	March 1980
	6. Performing Organization Code: --
7. Author(s): E. W. Saaski and J. H. Hartl	8. Performing Organization Report No.: None
9. Performing Organization Name and Address: Sigma Research, Inc. 2950 George Washington Way Richland, WA 99352	10. Work Unit No.: --
	11. Contract or Grant No.: NAS3-21202
12. Sponsoring Agency Name and Address: National Aeronautics and Space Administration Washington, DC 20546	13. Type of Report and Period Covered: Contractor Report
	14. Sponsoring Agency Code: --

15. Supplementary Notes

Final Report: Project Manager, Louis Gedeon, Physics and Electronics Division, NASA Lewis Research Center, Cleveland, Ohio

16. Abstract

Several two-phase heat transfer fluids were tested in aluminum and carbon steel reflux capsules for over 25,000 hours at temperatures up to 300°C. Results of these tests are presented. Several fluids showed very good stability and would be useful for long duration heat transfer applications over the range 100°C to 350°C.

Instrumentation for the measurement of surface tension and viscosity were also constructed for use with heat transfer fluids over the temperature range 0° to 300°C and with pressures from 0 to 10 atmospheres. The surface tension measuring device constructed requires less than a 1.0 cc sample and displayed an accuracy of ±5% in preliminary tests, while the viscometer constructed for this program requires a 0.050 cc sample and showed an accuracy of about ±5% in initial tests.

17. Key Words (Suggested by Author(s))	18. Distribution Statement
Heat Pipes Material compatibility Corrosion Decomposition	Unclassified-Unlimited STAR Category 34

19. Security Classif. (of this report)	20. Security Classif. (of this page)	21. No. of Pages	22. Price*
Unclassified	Unclassified	57	

* For sale by the National Technical Information Service, Springfield, Virginia 22161

NASA-C-168 (Rev. 10-75)

N80-23599#

NASA CR 159847

TWO-PHASE WORKING FLUIDS FOR THE TEMPERATURE RANGE 50-350°C (PHASE II)

E. W. Saaski

J. H. Hartl

Prepared Under Contract No. NAS3-21202
by
Sigma Research, Inc.
2950 George Washington Way
Richland, Washington 99352
for
LEWIS RESEARCH CENTER
National Aeronautics and Space Administration
Cleveland, Ohio

May 1980

Abstract

Twelve two-phase heat transfer fluids were tested in aluminum and carbon steel reflux capsules for over 25,000 hours at temperatures up to 300°C. Results of these tests are presented. Several fluids showed very good stability, and would be useful for long duration heat transfer applications over the range 50 to 350°C.

Instruments for the measurement of surface tension and viscosity were also constructed for use with heat transfer fluids over the temperature range 0 to 300°C and with pressures from 0 to 10 atmospheres. The surface tension measuring device constructed requires less than a 1.0 cc sample and displayed an accuracy of ±5% in preliminary tests, while the viscometer constructed for this program requires a 0.050 cc sample and also showed an accuracy of about ±5% in initial tests.

CONTENTS

FIGURES

TABLES

1.0 INTRODUCTION

This program extends investigations initiated in an earlier search (NAS3-20222) for thermally stable two-phase working fluids for the temperature range 100 to 400°C.

The application of heat pipes to thermal transport processes in this temperature range has been hindered for some time by the lack of suitable fluid-envelope combinations capable of long-term compatibility and integrity. In the previous NASA program, a number of potentially promising fluids were identified and are currently undergoing compatibility testing at Sigma Research, Inc. In addition to these fluids identified and placed in test, a very promising family of fluids, the halogenated aromatic hydrocarbons, was recognized. With the addition of a halogen constituent, ring compounds take on a number of desirable properties not found in the normal aromatic hydrocarbons. For this reason, it appeared desirable to subject these fluids to the same type of rigorous testing program already in progress.

In the case of many of the halogenated aromatics, as well as for a number of other working fluids, it is clear that fluid property data in the temperature range 100 to 300°C are often inadequate or completely lacking. Since heat pipe function is greatly affected by fluid properties such as viscosity and surface tension, it is imperative that accurate values for these properties be determined. Due to the vapor pressures and temperatures involved in this operating range, special measurement devices are required, and instruments were constructed to measure these properties over the temperature range 0 to 300°C and to pressures of 10 atmospheres.

2.0 TECHNICAL RESULTS

In this section, program results are discussed in detail. Three basic tasks were performed in this program. The first task, discussed in Section 2.1, was a further investigation of intermediate-temperature (100 to 350°C) working fluids, and specifically, the halogenated aromatic hydrocarbons, using a test stand constructed under Contract NAS3-20222 (report 135255).[1]

The second task was to build and deliver to Lewis Research Center devices for measuring, over a wide range of temperatures and pressures, working fluid viscosity and working fluid surface tension. In the search for new heat pipe working fluids, it has become quite clear that many potentially interesting fluids have totally unknown viscosities and surface tension, yet these physical properties are of first-order importance to heat pipe function. In this section, the theoretical bases for these instruments are developed. A more device-oriented discussion is presented in the corresponding User's Manuals.

The third task was a culmination of the working fluid studies in that two heat pipes were built and charged with appropriate intermediate-temperature working fluids. These pipes were then delivered to Lewis Research Center and are suitable for use as either demonstration heat pipes or life test heat pipes.

2.1 Halogenated Aromatic Compounds

In the previous working fluid study program (NAS3-20222), it was shown that ring-structured aromatic hydrocarbons are much more thermally stable than straight-chain hydrocarbons. Naphthalene, for example, was identified as a comparatively stable organic working fluid for the intermediate temperature range with a melting point of 80.1°C and a boiling point of 218°C. Other potential aromatic working fluids include diphenyl (b.p. = 255°C) and the terphenyls (b.p. = 332 - 405°C).

An unfortunate disadvantage of these fluids is that they are solids at room temperature, and the start-up of such heat pipes could conceivably lead to a freeze-out phenomenon wherein the working fluid condenses and freezes in the condenser instead of remaining a liquid and returning to the evaporator. It would be desirable for a heat pipe working fluid to be a liquid over a wide temperature range to minimize this possible problem, but without sacrificing thermal stability.

Halogenated aromatic hydrocarbons are of interest in this context, particularly the fluorinated compounds. As shown in Table 2.1-1, the carbon-fluorine bond is actually somewhat stronger than the carbon-hydrogen bond, indicating that fluorinated ring-structure compounds should be quite stable. A clear example of this is the fluid hexafluorobenzene (C_6F_6).

This material has a melting point of 5°C and a boiling point of 80.25°C, and is considered to be thermally stable to a temperature of 650°C.[2] Various physical properties are summarized in Table 2.1-2. The liquid density at 25°C is 1.61 g/cm^3. The vapor pressure of hexafluorobenzene at various temperatures is given by the relation of Table 2.1-2. If a pressure of 15 atmospheres is considered the maximum safe working pressure, then this fluid is usable up to 195°C. Other possible halogenated aromatics include the fluoro- and chloro-napthalenes. The Koppers Company of Pittsburgh, Pennsylvania, made a wide range of chlorinated napthalene materials that were used in such varied applications as sludge removal additives in petroleum oils and as high quality dielectric liquids and waxes.[3] The melting and boiling points of these materials are presented in Figure 2.1-1 as a function of chlorination level. It is quite remarkable that the addition of 1 chlorine molecule to napthalene drops the melting point of the material from 80.1 (pure napthalene) to -25°C (mono-chloronapthalene), while the boiling point goes from 218 to 250°C. Dichloronapthalene, on the other hand, has a melting point of about 60°C, and in this respect is similar to pure napthalene. These materials were relatively inexpensive, costing on the order of $1.00/lb. Unfortunately, Koppers Company halted production of these materials during 1977 because of excessive costs in

Table 2.1-1

BOND DISSOCIATION ENERGIES FOR VARIOUS WORKING FLUID VAPORS (Kcal/mole)[1]

	H	CH_3	C_2H_5	CHO	OH	F	Cl	Br	I	NH_2	C	C_2H
H	104	104	98	-79	119	136	103	88	71	104	120	
CH_3	104	88	85	71-75	88	108	84	70	56	79	105-110	
C_2H	<121	-110	-109									
C_2H_3	104	92	-90	-84			84		-55		-121	
CH_3CO	89	81	83	-59	110	119	79	-67	-51	-98		
C_2H_5	98	85	85	-71	90		81	69	53	78		
C_2H_5O	102	80	82		42							
$n\text{-}C_3H_7$	98	85	79	-71			82	69	50	77		-106
$i\text{-}C_3H_7$	95	84	-75		92	106	81	68	.53	85		-103
$n\text{-}C_4H_9$	94	78	78									
$i\text{-}C_4H_9$	91	80			91		79	63	50	84		
C_6H_5	112	93	94	-83	96	125	86	70-72	61	-94	-124	-119
$C_6H_5CH_2$	85	70	68		77		68	51	38	59	-95	
$C_{10}H_7$								70				
$C_{10}H_7\text{-}CH_2$	-76											

1) Variations of ± 10 Kcal/mole are not uncommon among different investigators.

meeting OSHA plant-site regulations[4] and Koppers Company was the only U.S. company manufacturing the pure chlorinated napthalenes on a production basis. However, Mobay Chemical Corporation manufactures some chlorinated napthalene mixtures, and the materials are still available from chemical supply houses.

Because of the unusual melting point depression with mono-chloronapthalene it could be expected that monofluoronapthalene would show similar behavior. This has been found to be correct--the melting point of 1-fluoronapthalene is -9°C and its boiling point is 216°C. It was also found that the melting point of octafluoronapthalene ($C_{10}F_8$) is 87-88°C, which is much lower than a value of 185°C for octachloronapthalene. Octafluoronapthalene is, of course, nonflammable. The fluorinated napthalenes have not been commercialized but are available as relatively expensive reagents from chemical supply houses. For example, 25 grams of octafluoronapthalene cost $45.00.

Table 2.1-2

PHYSICAL PROPERTIES OF HEXAFLUOROBENZENE[1]

Formula	- C_6F_6
Molecular weight	- 186.06
Freezing point	- +5°C
Boiling point	- +80.25°C
Critical point	- 243.2 0.4°C
Critical pressure	- 32.05 0.71 atm
Heat of vaporization at boiling point = 32,700 J/g-mole	
Surface tension	- = 24.62 - 0.113T (dynes/cm, °C)
Viscosity at boiling point = 0.43 centipoise	
Specific gravity	- 1.61 g/cm^3 at 25°C
Vapor pressure	- $\log_{10}$ (P) = 4.37835 - 1386.88/(T + 238.03) (atm, °C)
Stability	- thermally stable at over 650°C
Toxicity	- medium lethal air concentration for mice/2 hrs = 95 mg/liter

[1]Derived from Reference 2.

The discussion presented in this section documents the unusual properties of halogenated aromatic compounds. Hexafluorobenzene, for example, is thermally stable to 650°C, while monochloronapthalene has a remarkably low melting point of -25°C. These halogenated aromatic compounds possess a great deal of the thermal stability associated with the benzene ring structure, while displaying other favorable properties such as a wide liquid-phase range.

2.1.1 Reflux Tests

Thirteen working fluids have been installed in mild steel (A-178) and aluminum (6061) heat pipes and operated continuously in reflux for total elapsed times up to 28,000 hours. Heat pipe design, cleaning procedures, and testing protocol are described in detail in the final report for NAS3-20222 (report CR-135255). Table 2.1-3 outlines principal characteristics of the heat pipes used. Heat pipe function during operation was monitored using three ±2°F limit type K thermocouples per heat pipe. The thermocouples were placed at the center of the evaporator and adiabatic sections,

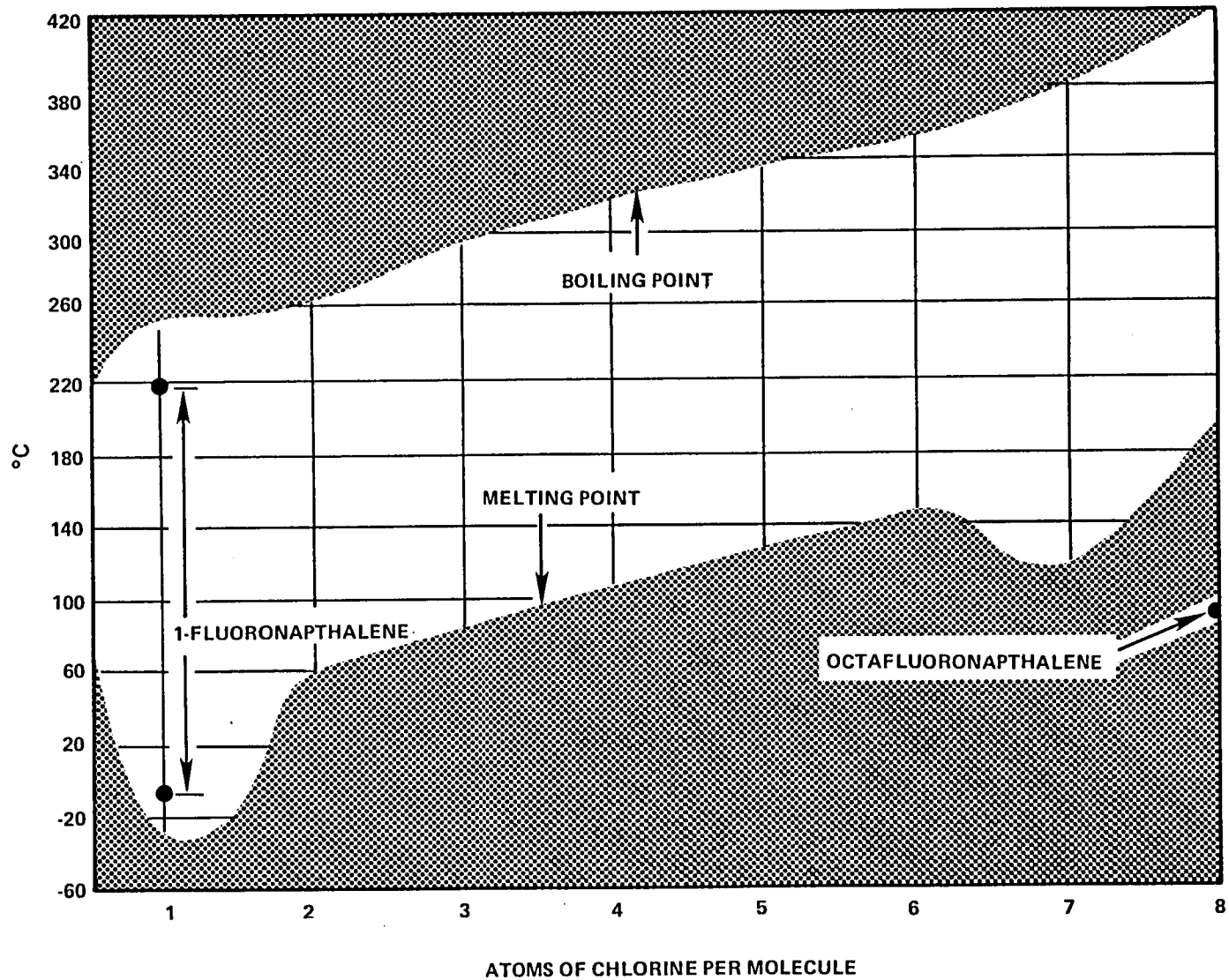

Figure 2.1-1. The Melting and Boiling Points for Chlorinated Napthalene Compounds As a Function of Degree of Chlorination. Similar Data for 1-Fluoronapthalene and Octafluoronapthalene are Presented for Purposes of Comparison.

Table 2.1-3

HEAT PIPE DESIGN SUMMARY

Parameter	Value	
	Aluminum	Steel
Material	6061	A-178
Physical dimensions		
Diameter (I.D./O.D.), cm	1.26/1.588	1.26/1.588
Evaporator length, cm	15.25	15.25
Adiabatic length, cm	15.25	15.25
Condenser length, cm	15.0	14.0
Wicking (evaporator only)	100 mesh, 1100 series alloy	200 mesh, 304 stainless alloy

and 1.25 cm below the condenser blind end, respectively, and were monitored with a Doric Digitrend data logger with 0.1°C resolution. The following sections discuss the test results for these various fluids. Table 2.1-4 is a summary of these tests, and Figure 2.1-2 shows time dependence of the adiabatic-condenser temperature difference for several fluids of interest.

Table 2.1-5 is a detailed summary of measured heat pipe evaporator-adiabatic $\left(\Delta T_{ea}\right)$ and adiabatic-condenser $\left(\Delta T_{ac}\right)$ temperature differences as a function of time for those fluid/envelope combinations that showed relatively modest changes in performance over the life test period.

Organic Fluids

All organic fluids tested with the exception of carbon disulphide were aromatic in structure, and on this basis, can be expected to exhibit low noncondensable gas generation rates compared to straight-chain hydrocarbons. Carbon disulphide would be expected to have an essentially zero generation rate because of the absence of potentially gaseous species in the compound.

Table 2.1-4

REFLUX DATA SUMMARY

Working Fluid (Boiling Point, °C)	Envelope[1]	Operating Time (hr)/Temp (°C)	Heat Input (Watts)	Average $\Delta T_{ea}^2/\Delta T_{ac}^2$	Comments
CS_2 (46.5°)	Al	28,540/62	7.0	0.8/1/1	small increase in ΔT_{ea}, ΔT_{ac}
	C.S.	28,540/58	6.4	0.4/0.1	stable operation
Toluene(110.4°)	Al	23,130/137	26.2	3.1/2.6	stable operation
	C.S.	700/119	26.0	1.6/4.1	heat pipe leak - failed
Napthalene(217.9°)	Al	27,750/215	52.5	12.5/4.3	stable operation
	C.S.	6,430/217	65.0	3.0/3.4	burn-out on re-start
Biphenyl(255°)	Al	8,000/241	--	24.1/--	wick movement, evap. - failed
	C.S.	24,400/253	80.0	4.4/102.0	stabilized gas leg
0-Terphenyl(332°)	Al	672/290→308	78.0	7.8/67.4	rapid increase in NCG[3]
	C.S.	27,750/272	71.0	10.0/51.5	stabilized gas leg
Tin Tetrachloride(114.1°)	Al	--/159	--	--	incompatible
	C.S.	27,750/156	26.0	4.0/9.7	stable operation
Titanium Tetrachloride(136.4°)	Al	2,500/165	30.0	6.0/7.2	sudden burn-out/wick corr.
	C.S.	28,540/159	39.0	4.1/1.7	stable operation
Antimony Trichloride(219.0°)	Al	--/227	--	--	incompatible
	C.S.	5,000/203	40.0	6.3→169/62	incompatible-rising ΔT_{ea}
Suntech Fluorocarbon "R"(190°)	Al	13,380/209	38.0	11.0/15.6	gradual increase in NCG[3]
1-Fluoronapthalene(216°)	Al	13,380/220	39.5	5.8/36.0	gradual increase in NCG[3]
	C.S.-1	4,790/216	56.0	5.0/57.0	stable operation
	C.S.-2	26,370/257	70.0	7.4/4.3	stable operation
Octafluoronapthalene(---°)	Al	13,400/215	36.5	4.3/3.4	stable operation
	C.S.	13,400/209	33.0	4.5/90.0	stable gas leg
Monochloronapthalene(250°)	C.S.	642/266→306	--	--	incompatible

(1) Al = 6061 aluminum, C.S. = A-178 carbon steel

(2) ea = evaporator-adiabatic temperature difference; ac = adiabatic-condenser temperature difference

(3) NCG = noncondensable gas

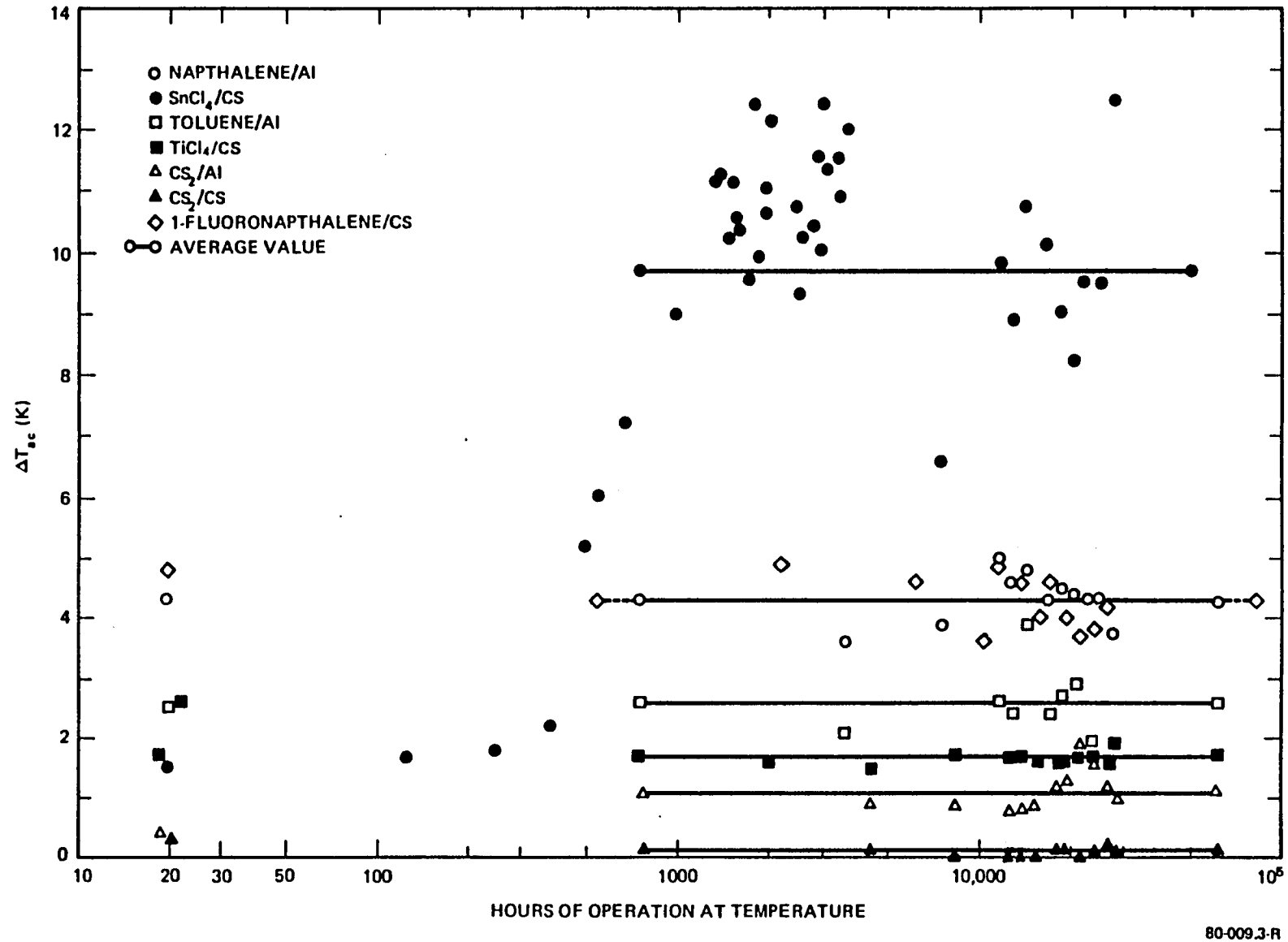

Figure 2.1-2. Heat Pipe Adiabatic-Condenser Temperature Differences.

Table 2.1-5

LIFE TEST DATA LOG

Heat Pipe	Operating Temp.	Elapsed Time (hr)	T_{ad}	ΔT_{ea}	ΔT_{ac}
NAPTHALENE/AL, 76-1	215°C	3,573	216.9	11.3	3.6
		7,560	216.5	12.9	3.9
		11,830	215.0	13.7	5.0
		12,890	216.5	12.2	4.6
		14,350	214.6	11.9	4.8
		17,130	215.8	11.8	4.3
		18,810	216.8	11.7	4.5
		20,900	216.7	12.4	4.4
		23,130	213.3	12.4	4.3
		25,875	215.2	13.7	4.3
		27,750	212.1	13.7	3.7
Average Value				<12.5>	<4.3>
$SnCl_4$/C.S., 76-11	156°C	3,573	158.3	3.4	12.0
		7,560	158.2	4.5	6.7
		11,830	154.7	4.1	9.8
		12,890	155.6	4.5	8.9
		14,350	153.5	4.4	10.7
		17,130	155.7	4.1	10.1
		18,810	157.9	3.9	9.0
		20,900	159.7	3.8	8.2
		23,130	155.6	4.0	9.5
		25,875	157.7	3.8	9.5
		27,750	153.5	3.7	12.4
Average Value				<4.0>	<9.7>
TOLUENE/AL, 76-8	137°C	3,573	131.3	3.2	2.1
		7,560	--	--	--
		11,830	132.9	3.0	2.6
		12,890	140.5	3.1	2.4
		14,350	138.6	1.4	3.9
		17,130	139.8	4.1	2.4
		18,810	140.2	4.1	2.7
		20,900	137.4	3.1	2.9
		23,130	134.7	3.0	1.9
		25,875	--	--	--
		27,750	--	--	--
Average Value				<3.1>	<2.6>

Table 2.1-5 (continued)

LIFE TEST DATA LOG

Heat Pipe	Operating Temp.	Elapsed Time (hr)	T_{ad}	ΔT_{ea}	ΔT_{ac}
$TiCl_4$/C.S., 76-9	159°C	4,365	156.0	4.5	1.5
		8,349	158.6	3.4	1.7
		12,621	158.3	3.9	1.7
		13,680	160.0	4.2	1.7
		15,150	156.1	4.4	1.5
		17,925	158.1	4.2	1.6
		19,600	159.9	4.3	1.6
		21,700	162.4	4.7	1.6
		23,925	161.8	4.0	1.7
		26,670	160.8	4.0	1.6
		28,540	159.2	3.1	2.0
Average Value				<4.1>	<1.7>
CS_2/C.S., 76-13	58°C	4,365	59.9	0.3	0.1
		8,349	58.4	0.4	-0.1
		12,621	58.2	0.4	0.0
		13,680	57.0	0.3	0.0
		15,150	56.8	0.4	0.1
		17,925	58.2	0.4	0.1
		19,600	59.0	0.4	0.1
		21,700	59.1	0.4	0.1
		23,925	59.3	0.4	0.1
		26,670	58.4	0.4	0.2
		28,540	57.9	0.8	0.1
Average Value				<0.4>	<0.1>
CS_2/Al, 76-14	62°C	4,365	61.7	0.3	0.9
		8,349	61.8	0.5	0.9
		12,621	61.3	0.6	0.8
		13,680	61.5	0.5	0.8
		15,150	60.3	1.9	0.9
		17,925	61.0	0.9	1.2
		19,600	62.6	0.8	1.3
		21,700	63.2	0.7	1.9
		23,925	63.6	0.8	1.6
		26,670	62.8	1.2	1.2
		28,540	62.2	1.0	1.0
Average Value				<0.8>	<1.1>

Table 2.1-5 (continued)

LIFE TEST DATA LOG

Heat Pipe	Operating Temp.	Elapsed Time (hr)	T_{ad}	ΔT_{ea}	ΔT_{ac}
1-FLUORONAPTHALENE/ C.S., 77-18	257°C	2,201	263.2	6.9	4.9
		6,185	266.5	6.8	4.6
		10,460	258.1	8.4	3.6
		11,510	256.0	6.9	4.9
		12,980	256.2	7.5	4.6
		15,761	253.9	7.5	4.0
		17,440	255.3	7.6	4.6
		19,531	255.6	7.7	4.0
		21,760	252.6	7.4	3.7
		24,500	254.5	7.4	3.8
		26,370	252.3	7.2	4.2
Average Value				<7.4>	<4.3>
0-TERPHENYL/C.S., 76-3	272°C	3,573	278.1	9.4	43.6
		7,560	275.7	10.1	49.5
		11,830	272.8	11.2	52.3
		12,890	272.0	10.1	49.8
		14,350	272.5	9.9	48.4
		17.130	270.9	10.0	51.5
		18,810	271.4	10.1	51.2
		20,900	272.3	10.2	51.5
		23,130	268.4	9.8	57.2
		25,875	269.5	10.0	55.0
		27,750	268.1	9.7	56.4
Average Value				<10.0>	<51.5>
SUNTECH FLUOROCARBON "R"/AL, 78-24	211°C	0	194.8	11.3	5.2
		7	208.9	10.2	8.2
		25	205.5	10.6	7.3
		51	193.9	17.1	7.7
		121	196.5	10.8	8.2
		166	206.9	10.4	7.5
		191	208.9	10.1	7.8
		310	210.4	10.1	8.1
		502	214.7	9.6	9.1
		670	216.8	9.0	8.4
		790	212.5	9.1	9.0
		1,030	218.9	8.6	8.9
		1,222	210.2	9.5	11.8
		1,390	211.9	10.0	13.6
		1,630	218.6	10.1	13.4
		1,966	210.6	11.0	16.7

Table 2.1-5 (continued)

LIFE TEST DATA LOG

Heat Pipe	Operating Temp.	Elapsed Time (hr)	T_{ad}	ΔT_{ea}	ΔT_{ac}
SUNTECH FLUOROCARBON "R"/AL, 78-24 (cont.)		2,319	212.3	11.3	17.4
		2,693	209.9	11.4	19.3
		2,963	210.3	11.4	20.3
		3,807	216.8	11.0	20.4
		4,071	214.0	11.4	19.9
		4,287	216.1	11.2	20.3
		5,127	217.3	11.1	22.4
		5,583	211.8	11.7	26.3
		5,963	213.8	11.6	24.0
		6,580	211.3	12.0	21.5
		8,240	213.8	12.1	24.6
		9,320	214.0	12.2	25.2
		11,560	214.6	12.3	26.1
		13,380	209.1	12.6	29.4
Average Value				<11.0>	<15.6>
OCTAFLUORONAPTHALENE/ C.S., 78-20	209°C	22	177.8	4.5	15.9
		24	185.5	4.9	8.7
		31	183.7	4.7	10.7
		75	157.2	4.4	36.9
		145	160.7	4.5	34.6
		190	188.3	4.4	8.3
		215	186.3	4.7	10.3
		334	185.6	4.7	9.8
		526	207.2	4.9	--
		694	214.2	4.8	--
		814	212.5	4.7	--
		1,054	203.5	4.6	--
		--	--	--	--
		1,414	205.6	4.6	--
		1,654	209.0	4.8	--
		1,990	207.6	4.4	--
		2,343	204.2	4.4	--
		2,717	205.5	4.3	--
		2,987	207.1	4.6	--
		3,831	215.1	4.6	101.3
		4,095	214.0	4.4	101.6
		4,311	215.7	4.4	99.1
		5,151	215.4	4.7	91.4
		5,600	214.2	4.5	90.1
		5,980	205.6	4.4	77.9
		6,600	213.0	4.6	86.3

Table 2.1-5 (continued)

LIFE TEST DATA LOG

Heat Pipe	Operating Temp.	Elapsed Time (hr)	T_{ad}	ΔT_{ea}	ΔT_{ac}
OCTAFLUORONAPTHALENE/		--	--	--	--
C.S., 78-20 (cont.)		9,340	204.7	4.3	80.0
		11,580	206.5	4.1	86.7
		13,400	204.5	4.0	97.0
Average Value				<4.5>	
1-FLUORONAPTHALENE/C.S.,	216°C	15	211.6	5.3	70.8
78-22		17	220.1	5.5	60.3
		24	217.6	5.5	67.0
		68	209.0	5.2	70.7
		138	210.3	5.3	68.0
		183	219.8	5.6	53.5
		208	219.7	5.2	53.4
		327	217.5	5.2	54.1
		519	220.2	5.1	52.9
		687	215.4	4.9	55.0
		807	216.3	4.8	53.8
		1,047	216.8	4.8	56.2
		1,239	217.5	4.8	53.3
		1,407	215.4	4.9	52.8
		1,647	217.8	5.0	54.6
		1,983	214.0	4.7	56.4
		2,336	214.2	4.8	56.9
		2,710	215.2	4.9	54.9
		2,980	216.7	4.7	54.6
		3,824	215.6	4.7	56.8
		4,088	215.2	4.8	55.2
		4,304	216.3	4.8	55.7
		4,784	212.0	4.5	61.3
		4,790	-------HEATER FAILED------		
Average Value				<5.0>	<57.0>
1-FLUORONAPTHALENE/AL,	220°C	0	219.7	3.9	25.0
78-23		7	221.4	4.1	25.4
		25	218.1	4.2	28.4
		51	201.4	4.0	31.2
		121	203.8	4.2	31.0
		166	216.8	5.3	28.6
		191	218.3	4.8	29.8
		310	217.7	4.9	28.2
		502	221.0	5.0	28.8
		670	223.6	4.9	28.1

Table 2.1-5 (continued)

LIFE TEST DATA LOG

Heat Pipe	Operating Temp.	Elapsed Time (hr)	T_{ad}	ΔT_{ea}	ΔT_{ac}
1-FLUORONAPTHALENE/AL, 78-23 (cont.)	220°C	790	218.3	5.0	30.7
		1,030	225.0	5.2	30.0
		1,222	218.7	5.1	32.6
		1,390	215.9	6.5	34.6
		1,630	223.7	5.4	34.8
		1,966	218.3	6.6	37.4
		2,319	220.2	6.4	38.2
		2,693	222.3	5.4	37.0
		2,963	224.3	5.7	38.1
		3,807	221.9	7.2	39.9
		4,071	221.8	7.1	39.7
		4,287	223.2	7.2	39.2
		5,127	225.8	5.5	40.4
		5,583	223.1	7.2	41.8
		5,963	221.3	7.3	42.3
		6,580	223.9	6.8	41.2
		8,240	219.3	6.9	49.1
		9,320	218.2	6.8	50.3
		11,560	223.8	7.3	49.6
		13,380	221.2	7.3	49.5
Average Value				<5.8>	<36.0>
OCTAFLUORONAPTHALENE/AL 78-21	215°C	15	204.7	4.3	3.5
		17	217.2	4.5	3.5
		24	214.5	4.5	3.6
		42	215.6	4.5	3.3
		68	206.5	4.2	4.8
		138	209.0	4.2	3.6
		183	218.1	4.3	3.4
		208	219.7	4.3	3.8
		327	216.9	4.4	3.1
		519	221.6	4.3	3.4
		687	216.5	4.1	3.9
		807	218.6	4.4	3.2
		1,047	220.7	4.5	3.3
		1,239	219.4	4.4	4.2
		1,407	218.1	3.8	3.7
		1,647	223.2	3.9	3.5
		1,983	219.8	4.1	3.2
		2,336	221.3	4.1	3.0
		2,710	221.1	4.1	3.3
		2,980	220.0	4.1	3.1
		3,824	214.3	4.2	3.1

Table 2.1-5 (continued)

LIFE TEST DATA LOG

Heat Pipe	Operating Temp.	Elapsed Time (hr)	T_{ad}	ΔT_{ea}	ΔT_{ac}
OCTAFLUORONAPTHALENE/AL 78-21 (cont.)	215°C	4,088	215.5	4.3	2.9
		4,304	215.0	4.5	2.9
		5,144	216.1	4.6	2.7
		5,600	214.5	4.6	2.8
		5,980	213.0	4.8	3.5
		6,600	214.3	4.8	2.7
		8,260	210.7	4.4	3.7
		9,340	207.6	4.3	3.6
		11,580	207.3	4.3	3.3
		13,400	204.0	4.2	3.5
Average Value				<4.3>	<3.4>

Fluid/envelope combinations that exhibited high stability, i.e., no substational change in operating temperature with time, included

- CS_2/C.S.: 28,540 hr @ 58°C
- Toluene/Al: 23,130 hr @ 137°C
- Napthalene/Al and C.S.: 27,750 hr @ 215°C

Both biphenyl and O-terphenyl in carbon steel heat pipes exhibited noncondensable gas generation, but the gas evolution either tapered off in each case, or a dynamic equilibrium was achieved whereby the gas production rate was balanced by gas permeation through the heat pipe wall.

Inorganic Fluids

Of the inorganic fluids, two combinations have demonstrated satisfactory long-term stability

- Titanium tetrachloride/C.S.: 28,540 hr @ 159°C
- Tin tetrachloride/C.S.: 27,750 hr @ 156°C

On the basis of relative decomposition potentials, titanium tetrachloride would be expected to be stable in a steel envelope, but tin tetrachloride and ferric chloride have very similar decomposition potentials, and the outcome of a $SnCl_4$/Fe heat pipe combination cannot be predicted with certainty from decomposition potential data. The data and Figure 2.1-2 show stable operation after an initial burst of noncondensable gas generation following 500 hours of operation.

Chloro/Fluorocarbon Fluids

Four chloro- and fluorocarbon working fluids were tested in aluminum and steel heat pipes - 1-fluoronapthalene, octafluoronapthalene, monochloronapthalene, and Suntech fluorocarbon "R".[5] The latter compound is a proprietary trinary fluorinated ring compound that was developed for artificial blood purposes.

Of these fluids, three combinations show good stability

- 1-Fluoronapthalene/C.S.: 4,800 hr @ 216°C; 26,400 hr @ 257°C
- Octafluoronapthalene/Al: 13,400 hr @ 215°C
- Octafluoronapthalene/C.S.: 13,400 hr @ 209°C

The proprietary fluorocarbon "R" and 1-fluoronapthalene in aluminum heat pipes at 211°C and 220°C, respectively, have shown a continually falling condenser end temperature, indicating a slow build-up of noncondensable gas. Monochloronapthalene was found to react with the steel heat pipe envelope at 266°C and produce large amounts of noncondensable gas. Although the wall showed no visible deterioration, chemical analysis of the working fluid extracted from the heat pipe showed the presence of free chloride and ferric ions.

2.1.2 Post-Mortem Observations

Four heat pipes that failed since the Phase 1 report have been sectioned and examined to identify the cause of failure. The results of these examinations are presented in the following paragraphs.

Antimony Trichloride/Carbon Steel

This heat pipe failure over the period $5000 < t < 15{,}000$ hours was manifested by a gradual rise in the evaporator temperature, until at $t = 13{,}500$ hours, the adiabatic temperature had increased to 360°C from an initial 227°C. During this entire period, the adiabatic-condenser temperature difference had remained constant at about 60°C.

Examination of the heat pipe established that the working fluid had reacted with the stainless screen wick and had formed an amorphous solid mixture along the evaporator length that apparently caused evaporator working fluid starvation either through chemical consumption of working fluid or through a change in the wicking characteristics.

Biphenyl/Aluminum

The biphenyl/aluminum heat pipe operated for about 10,000 hours at 245°C before failing suddenly with a rapid rise in evaporator temperature. Examination of the heat pipe showed that the evaporator wick was lodged in the condenser zone. Because of periodic power failures at this facility, it is postulated that the wick was thrown into the condenser zone during violent boiling/vaporization associated with a heat pipe re-start. The smooth evaporator bore then led to fluid feed instabilities which resulted in burn-out.

Titanium Tetrachloride/Aluminum

This heat pipe failed after about 2500 hours at a temperature of 165°C. The failure mode of this heat pipe was similar to the previous biphenyl/aluminum and antimony trichloride/steel heat pipes in the respect that failure was manifested by a rapid rise in evaporator temperature. Examination of the heat pipe after sectioning showed severe degradation/corrosion/embrittlement of the heat pipe evaporator wick and a substantial annular deposit of aluminum trichloride at the condenser blind end. Failure is attributed to incomplete evaporator surface wetting.

The decomposition potential for aluminum trichloride is substantially greater than that of titanium tetrachloride, and hence production of aluminum trichloride could be expected from theoretical considerations. The annular deposit of aluminum trichloride at the condenser blind end is probably the result of vapor phase mass transfer of $AlCl_3$ formed in the evaporator. Aluminum trichloride is a solid at 165°C, and might be expected to precipitate out in the condenser during the condensation process.

Toluene/Carbon Steel

The evaporator rose rapidly in temperature after about 700 hours of operation at 119°C. The heat pipe interior was in very good condition upon examination, but no working fluid could be found. Heat pipe failure was apparently caused by a small leak that bled the working fluid from the heat pipe.

2.2 Surface Tension Measurement

Surface tension measurements are generally classified as static or dynamic. Static methods measure the surface tension of interfaces that have been quiescent for some time in contrast to dynamic methods, which generally rely on some periodic perturbation of the surface and hence tend to produce a degree of mixing at the interface. The measurement of surface tension by static means is performed in one of two ways.

In the first method, and the more accurate, the pressure difference across a curved interface is used along with total surface curvature to calculate surface tension. Common techniques of this type include the capillary height method, the maximum bubble pressure methods, the drop-weight method, and the method of sessile drops. The second method incorporates a solid surface that is used to produce an extended film of the fluid. Examples of this technique include the detachment of a ring or plate from a liquid surface and the measurement of soap solution surface tension by an extended film. These latter techniques are not applicable to heat pipe working fluids.

The dynamic methods rely on the perturbation of a liquid surface by some mechanism and a measurement of the subsequent restoring force produced by surface tension. Examples of dynamic methods include the measurement of surface ripple wavelength, the oscillations of jets from noncircular orifices, and the oscillations of pendant drops. Quantitative data are often difficult to obtain with the dynamic methods, and they were eliminated from consideration. It is worthwhile, however, to briefly describe the various static methods for surface tension measurement prior to discussing the method actually selected.

2.2.1 Capillary Rise-Height

In this method, the rise-height of liquid in a capillary tube is used to calculate the surface tension. For very small diameter tubes, the surface tension is given by

$$\gamma \cos \theta = \tfrac{1}{2} g r h \left(\rho_f - \rho_v \right) \qquad 2.2\text{-}1$$

where: γ = surface tension,

θ = the wetting angle,

r = the capillary radius,

h = the rise-height, and

ρ_f and ρ_v = the fluid and vapor density.

The factor g is gravitational acceleration. Where the contact angle deviates from zero, the true surface tension cannot be obtained unless θ is independently measured. This is generally difficult and is an inherent problem with the capillary rise-height method. The rise-height equation is also only correct if the reference surface is perfectly planar. This generally requires a reservoir on the order of 2.5 cm diameter, into which the capillary is inserted.

2.2.2 Maximum Bubble Pressure Method

If a small orifice is submerged in a liquid and a gas is forced out of the orifice, it will be seen that the necessary gas pressure for bubble evolution is a maximum at the point that the developing bubble is a perfect hemisphere. At this point the partial pressure of noncondensable gas in the bubble is

$$P_{gb} = P_{gv} + \left(\rho_f - \rho_v\right)gh + 2\gamma/r \qquad 2.2\text{-}2$$

where: P_{gb} = the gas partial pressure in the bubble,

P_{gv} = the gas pressure above the liquid, and

h = the depth of orifice submergence.

Note that in this case, in contrast to equation 2.2-1, the wetting angle is not a factor in the determination of the surface tension, γ. However, it is now necessary to measure relatively low pressure differences, on the order of 0.001 atm., a process that is difficult when the working fluid itself may be at a saturation pressure of several atmospheres.

2.2.3 Drop-Weight Method

A droplet will fall from a needle tip at a point such that the forces of surface tension are exceeded by droplet weight. The relationship between droplet weight and surface tension has been calculated and is tabulated; surface tension may be measured to an accuracy of about 0.1% by this technique. However, the measurement of drop weight for highly volatile working fluids appears to be a significant impediment to successful use of this technique for heat pipe working fluids.

2.2.4 Sessile Drop Method

If a liquid droplet or submerged gas bubble is carefully measured, it is possible to calculate the surface tension knowing only the maximum diameter of the droplet or bubble and the distance from this "equator" to the apex

of the droplet or bubble. This technique requires great care in measurement, minimal distortion by the surrounding fluid and sightports, and a measuring microscope.

2.2.5 Surface Tension Measurement: Selected Approach

Of the conventional approaches, the capillary rise-height method is the most simple and amenable to high pressure liquid/vapor systems. However, it does have a disadvantage in that the measurement of capillary prime height requires either a dimensionally long observation window or a means of remotely varying liquid height from a reference level. Since this must be done at a temperature on the order of 300°C and at a pressure of up to 10 atmospheres, it is not an easy feat.

A measurement technique that minimizes some of these problems is shown in Figure 2.2-1, and is based on the following argument. If a small amount of liquid is introduced into a tubular chamber of radius R_1, it is apparent that a circumferentially symmetric meniscus will form within the tube. The principal radii of curvature for this surface, r_a and r_b, are given by

$$r_a = \frac{(1 + U^2)^{3/2}}{dU/dx} \qquad 2.2\text{-}3$$

$$r_b = \frac{x\ (1 + U^2)^{1/2}}{U} \qquad 2.2\text{-}4$$

where: $U = dy/dx$, and the coordinate system is as shown in Figure 2.2-1. At $x = 0$, it is apparent from symmetry that $U = 0$, and that $r_a \equiv r_b \equiv R_o$.

The zone in the immediate vicinity of $x = 0$ is of parabolic cross section and will possess the optical properties of a parabolic mirror of focal length F and center radius R_o. The radius R_o is uniquely related to the fluid surface tension and fluid density for a fixed capsule radius. If a small beam of parallel light rays impinges at $x = 0$ and at some small angle with respect to the perpendicular, then the beam will be focused to a

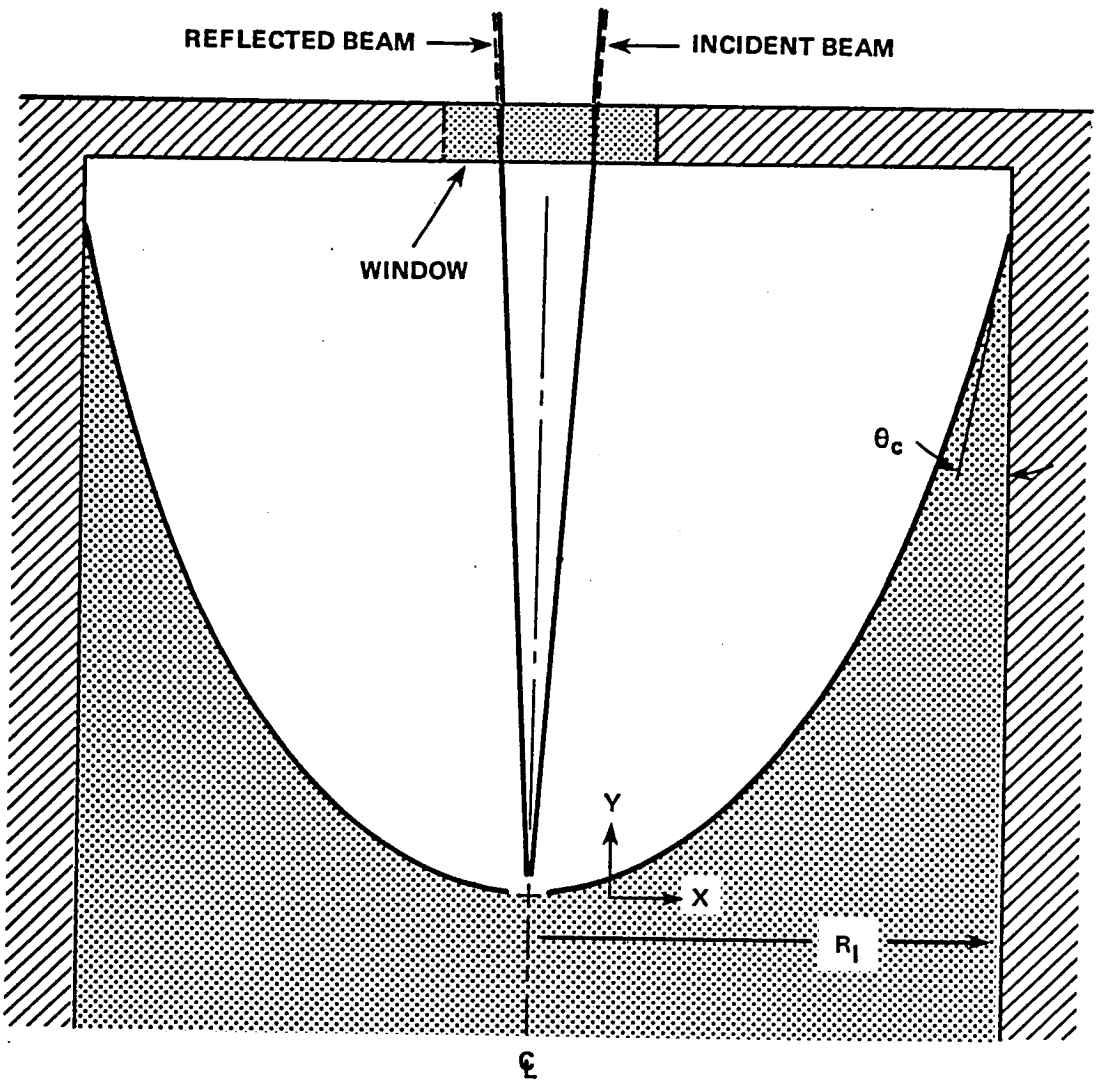

Figure 2.2-1. Schematic of Optical Beam Method for the Measurement of Surface Tension (θ_c = contact angle).

minimum diameter at the focal point F of the parabolic surface. The relationship of F to R_o is

$$F = \frac{R_o}{2} \qquad 2.2\text{-}5$$

The measurement of a particular sample's surface tension therefore consists of finding the distance from the fluid surface to the minimum reflected spot size, i.e., the liquid surface focal point, and then using this value to obtain the corresponding value of surface tension. The method is attractive because it requires only a small window at the top of the cell, and yields good accuracy since the focal length $R_o/2$ will generally be from several centimeters to a meter outside of the test chamber.

2.2.6 Theory

The modeling of capillary rise height phenomena sparked the interest of physicists before the turn of the century, and interest in this area continued thereafter for a long period. Bashforth and Adams calculated surface shapes for circumferentially symmetric menisci in 1883,[6] and these results were extended by Sugden in 1921.[7] This modeling of meniscus shape was originally derived to provide a second-order correction factor for capillary tube rise height methods of measuring surface tension, but as will be shown, the meniscus shape also provides an exceptionally elegant method of directly measuring surface tension.

The fundamental hydrostatic equation defining meniscus shape is

$$\gamma\left(\frac{1}{r_a} + \frac{1}{r_b}\right) = \Delta\rho g\left(y + \frac{2\gamma}{\Delta\rho g R_o}\right) \qquad 2.2\text{-}6$$

while the boundary conditions are

$$\frac{dy}{dx}(x = R_1) = \tan\left(\frac{\pi}{2} - \theta_w\right) \qquad 2.2\text{-}7$$

$$y(0) = 0 \qquad 2.2\text{-}8$$

$$\frac{dy}{dx}(0) = 0 \qquad 2.2\text{-}9$$

where: r_a and r_b are the principal radii of curvature at radial position "x" and vertical liquid/gas interfacial position "y" (see Figure 2.2-1). The local meniscus height y is measured with respect to the low point in the meniscus at position x = 0. The radius of curvature at the center x = 0 is R_o. The second equation is an identity which establishes the appropriate wetting angle at the cylinder wall, $x = R_1$. The factors γ, $\Delta\rho$, and g are respectively the surface tension, liquid-vapor density difference, and gravitational acceleration.

The equation 2.2-6 in Cartesian coordinates is equivalent to

$$\left(\frac{dU/dx}{(1 + U^2)^{3/2}} + \frac{U}{x(1 + U^2)^{1/2}}\right) = \frac{y_t}{a^2} \qquad 2.2\text{-}10$$

where: $U = dy/dx$, y_t is $\left(y + \frac{2\gamma}{\Delta\rho g R_o}\right)$ and $a^2 = \frac{\gamma}{\Delta\rho g}$.

Two approaches can be used to solve the ordinary differential equation 2.2-10. For small values of U on the order of 0.10 or less, terms which contain U^2 can be safely neglected, and as described by Lord Rayleigh, the resulting differential equation is[8]

$$\frac{dU}{dx} + \frac{U}{x} - \frac{y_t}{a^2} = 0 \qquad 2.2\text{-}11$$

The solution of this equation is the I_o modified Bessel function,

$$\frac{y_t}{\left(\frac{2\gamma}{\Delta\rho g R_o}\right)} = I_o(x/a) = 1 + \frac{1}{2^2}\left(\frac{x}{a}\right)^2 + \frac{1}{2^2 4^2} \cdot \left(\frac{x}{a}\right)^4 + \ldots \qquad 2.2\text{-}12$$

The relation given above is of use in starting the numerical calculations near x = 0, and will be referred to at a later point.

To solve the equation 2.2-10 for larger values of U, the equation was reformulated to the following coupled set of differential equations:

$$-\frac{dP}{dy^+} = y^+ - \frac{1}{x^+}\sqrt{1 - P^2} \qquad 2.2\text{-}13$$

$$\frac{dx^+}{dy^+} = P/\sqrt{1 - P^2} \qquad 2.2\text{-}14$$

where: $P = 1/\sqrt{1 + U^2}$; $x^+ = \frac{x}{a}$; $y^+ = \frac{y_t}{a}$.

Boundary conditions for these equations are

$$P = 1 \text{ and } x^+ = 0 \text{ @ } y^+ = 2\sqrt{B_0} \qquad 2.2\text{-}15$$

$$P = \cos\left(\frac{\pi}{2} - \theta_w\right) \text{ @ } x^+ = R_1/a \qquad 2.2\text{-}16$$

where: B_0 is the Bond number, $\gamma/\Delta\rho g R_o^2$.

The coupled equations 2.2-13 and 2.2-14 have been solved using Hamming's predictor-corrector technique for the differential equations $P' = F\left(P, y^+\right)$ and $x^{+\prime} = g(P)$. For the dependent variable P, the formulas used to estimate P_{n+1} from the prior calculated values are

$$P_{n+1} = P_{n-3} + \frac{4h}{3}\left(2P'_n - P'_{n-1} + 2P'_{n-2}\right) \qquad 2.2\text{-}17$$

Modifier:

$$m_{n+1} = P_{n+1} - \frac{112}{121}\left(P_n - P_n\right) \qquad 2.2\text{-}18$$

$$m'_{n+1} = F\left(m_{n+1},\ y^+_{n+1}\right) \qquad 2.2\text{-}19$$

Corrector:

$$C_{n+1} = \frac{1}{8}\left[9P_n - P_{n-2} + 3h\left(m'_{n+1} + 2P'_n - P'_{n-1}\right)\right] \qquad 2.2\text{-}20$$

Final value:

$$P_{n+1} = C_{n+1} + \frac{9}{121}\left(P_{n+1} - C_{n+1}\right) \qquad 2.2\text{-}21$$

The factor h is the step-size in y^+. The equations for x^+ are similar. This fourth-order predictor-corrector approach is not self-starting, i.e., values of the dependent variable and its first derivative are needed for respectively the previous 4 and 3 incremental positions in the independent variable y^+. These values have been generated by a fourth-order Runge-Kutta algorithm. The Runge-Kutta procedure in turn requires only information at one starting point. These x and y starting values are obtained from the Bessel function solution given earlier. The starting point is selected such that the Bessel function solution is appropriate; that is, dy/dx is much less than 1; the particular value of dy/dx selected is 0.017.

Table 2.2-1 summarizes the interrelationship of the four principal variables for zero contact angle.

B_o = Bond number based on meniscus radius at centerline

$= \gamma/\Delta\rho g R_o^2$

B_1 = Bond number based on tube radius

$= \gamma/\Delta\rho g R_1^2$

$\frac{R_1}{R_o}$ = Ratio of tube radius to central meniscus radius

$\frac{Y_{tm}}{a}$ = Dimensionless meniscus climb height

$= Y_{tm} \Big/ \sqrt{\gamma/\Delta\rho g}$

Y_{tm} = Vertical distance from center depression of meniscus to meniscus contact line, assuming zero contact angle

Table 2.2-1

PARAMETRIC SUMMARY TABLE FOR MENISCUS FORMATION IN A VERTICAL TUBE

B_o	B_1	R_1/R_o	$Y_{tm/a}$
1E-7	0.114165E-1	0.29596E-2	
1.5	0.119556E-1	0.35421E-2	
2	0.123618E-1	0.402229E-2	
3	0.129711E-1	0.48092E-2	
4	0.134315E-1	0.545717E-2	
5	0.138061E-1	0.601797E-2	
6	0.014124	0.651773E-2	
7	0.144017E-1	0.697176E-2	
8	0.014649	0.738995E-2	
9	0.148725E-1	0.77791E-2	
1E-6	0.150769E-1	0.814412E-2	1.49403
1.5	0.159049E-1	0.971136E-2	1.49634
2	0.165352E-1	0.109979E-1	1.49807
3	0.174905E-1	0.130966E-1	1.50064
4	0.182204E-1	0.148167E-1	1.50257
5	0.018819	0.162999E-1	1.50412
6	0.193308E-1	0.176178E-1	1.50543
7	0.197803E-1	0.188119E-1	1.50657
8	0.201826E-1	0.199093E-1	1.50759
9	0.020548	0.209284E-1	1.50850

Table 2.2-1 (continued)

PARAMETRIC SUMMARY TABLE FOR MENISCUS FORMATION
IN A VERTICAL TUBE

B_o	B_1	R_1/R_o	$y_{tm/a}$
1E-5	0.208835E-1	0.218826E-1	1.50933
1.5	0.022256	0.025961	1.51268
2	0.233153E-1	0.292883E-1	1.51520
3	0.249444E-1	0.346796E-1	1.51900
4	0.262082E-1	0.390671E-1	1.52188
5	0.272573E-1	0.428296E-1	1.52422
6	0.281629E-1	0.461569E-1	1.52622
7	0.028965	0.04916	1.52797
8	0.296884E-1	0.05191	1.52954
9	0.303497E-1	0.544558E-1	1.53095
1E-4	0.309605E-1	0.568324E-1	1.53225
1.5	0.334958E-1	0.669192E-1	1.53753
2	0.354924E-1	0.750667E-1	1.54159
3	0.386309E-1	0.881238E-1	1.54781
4	0.411226E-1	0.986256E-1	1.55261
5	0.432286E-1	0.107547	1.5566
6	0.450739E-1	0.115375	1.56004
7	0.467297E-1	0.122392	1.56308
8	0.482401E-1	0.128778	1.56583
9	0.049635	0.134656	1.56834
1E-3	0.509356E-1	0.140116	1.57066
1.5	0.564576E-1	0.162999	1.58031
2	0.609472E-1	0.18115	1.58794
3	0.682552E-1	0.209649	1.60002
4	0.742751E-1	0.232064	1.60969
5	0.795133E-1	0.250764	1.61793
6	0.842166E-1	0.266917	1.62521
7	0.885264E-1	0.281198	1.63178
8	0.925318E-1	0.294035	1.63782
9	0.962936E-1	0.305719	1.64343
0.01	0.998549E-1	0.316457	1.64869
0.015	0.115554	0.36029	1.67135
0.02	0.129004	0.393744	1.69018
0.03	0.152196	0.443975	1.72163
0.04	0.172492	0.481555	1.74825
0.05	0.191011	0.511629	1.77192
0.06	0.208309	0.536687	1.79356
0.07	0.224706	0.558138	1.81369
0.08	0.240407	0.576862	1.83264
0.09	0.25555	0.593449	1.85065

The present tabulation of menisci relations is substantially more extensive than any previous meniscus data tables in terms of both data density and overall range. This information has been curve-fitted and incorporated into the following surface-tension calculating algorithm:

$$\ell n\left(B_1\right) = -0.854857 + 1.64627\ \ell n\left(\frac{R_1}{R_o}\right) + 0.37662\left[\ell n\left(\frac{R_1}{R_o}\right)\right]^2 +$$

$$0.0500133\left[\ell n\left(\frac{R_1}{R_o}\right)\right]^3 + 0.00267328\left[\ell n\left(\frac{R_1}{R_o}\right)\right]^4 \qquad 2.2\text{-}22$$

when $0.003 \leq \left(\frac{R_1}{R_o}\right) \leq 0.2$

Computed values of B_1 using this equation are within ±0.5% of the value given in Table 2.2-1.

2.2.7 Accuracy of Technique

In the previous section, it was shown for small deviations from the tube axis that the liquid meniscus was described by the I_o Bessel function,

$$\frac{y_t}{\left(\frac{2\gamma}{\Delta\rho g R_o}\right)} = I_o(x/a) \qquad 2.2\text{-}23$$

Using this Bessel function solution, it is possible to calculate the surface orientation as a function of x/a (where $a^2 = \gamma/\Delta\rho g$), and determine the maximum radial zone over which the lens focal length is constant to within a given percentage error, $\pm\eta$. This information is of use in defining the maximum permissible input beam diameter, since larger beams will provide progressively more poorly defined focal points and will lead to increasingly large uncertainties in surface tension.

The fractional error in surface tension caused by an uncertainty ΔF in the focal point "F" is given by

$$\frac{1}{\gamma}\frac{d\gamma}{dF} \cdot \Delta F = \frac{-1}{B_1}\frac{dB_1}{dr^*} \cdot \frac{\Delta F}{F} \qquad 2.2\text{-}24$$

where

$$B_1 = \gamma/\Delta\rho g R_1^2 \text{ and } r^* = \frac{R_1}{R_o} \qquad 2.2\text{-}25$$

Focal point variation is calculated by evaluating the shift in intersection point of a reflected optical ray with the tube axis. For a local surface element having a tilt dy/dx with respect to the horizontal, the effective local focal length is

$$F_e = x/\tan\left[2 \text{ atan}\left(dy/dx\right)\right] \qquad 2.2\text{-}26$$

at x = 0,

$$F_e = F_o = R_o/2 \qquad 2.2\text{-}27$$

By monitoring the variation in F_e with radial position "x", the maximum value of x can be found such that the ratio $\Delta F/F_o$ does not exceed a fixed fraction, $\pm\eta$.

The relationship between uncertainty in focal length and uncertainty in surface tension is presented in Figure 2.2-2. Under typical use conditions, the range in Bond number B_1 will be from about 0.015 to 0.10, with a corresponding range in R_1/R_o of 0.008 to 0.30. In this range, if error in calculated surface tension is not to exceed ±1% (0.02 in $\Delta F/F$), then the ratio of light beam diameter to cup diameter should not exceed 0.064. Typical spot size for a small bench-scale laser is 0.8 to 1 mm and, hence, the

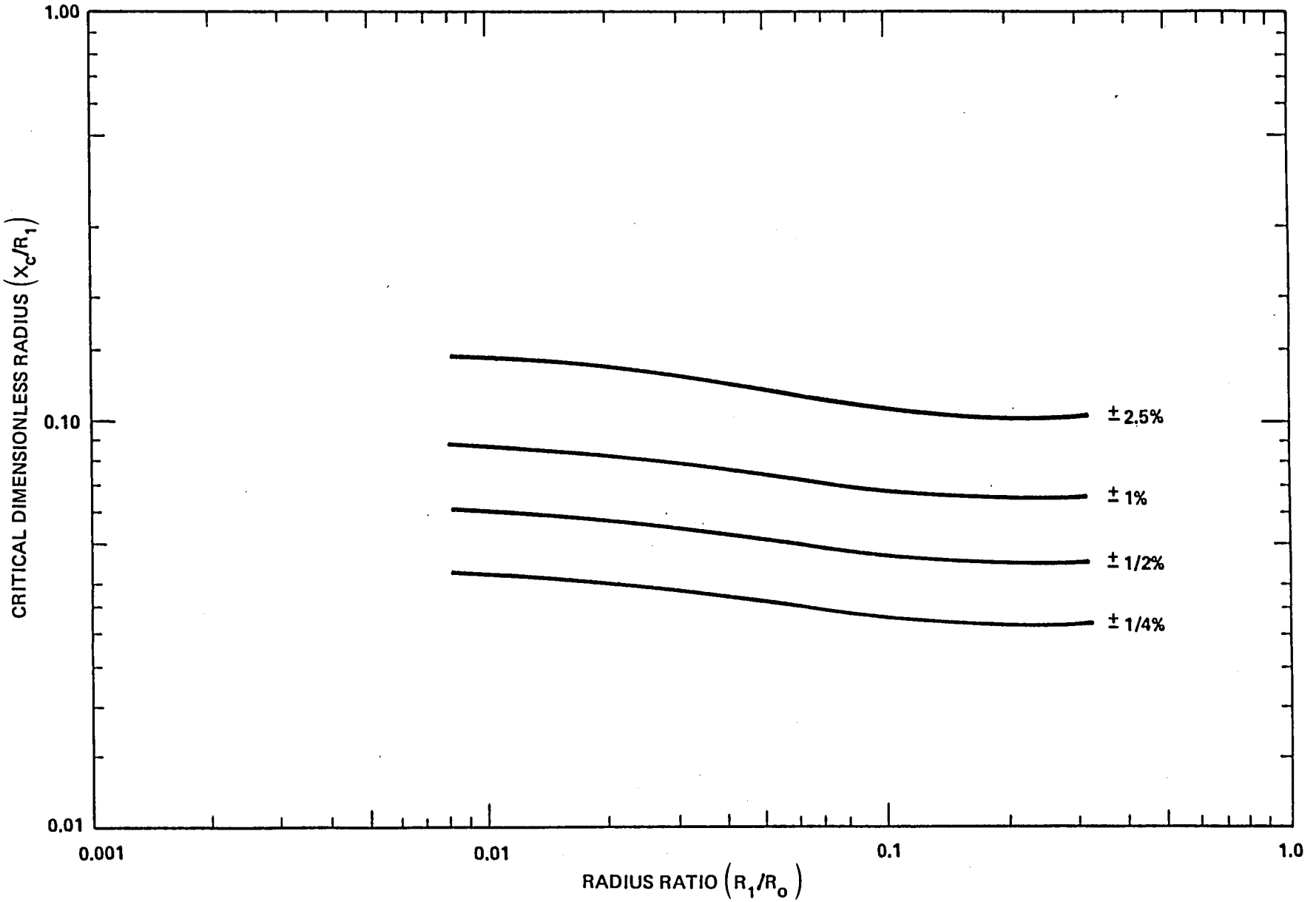

Figure 2.2-2. Critical Radius Ratio at Which Focal Length Variation Creates ±1/4%, ±1/2%, ±1%, and ±2.5% Uncertainties in Calculated Surface Tension.

liquid container diameter should be in the range of 1.25 to 1.56 cm. This is quite compatible with overall design considerations and, in fact, for a 2-cm-diameter cup, the maximum error attributable to a soft focus is about ±0.6% for a 1 mm laser beam.

2.2.8 Description of LRC Optical Tensiometer

The optical tensiometer is shown schematically in Figures 2.2-3 and 2.2-4. A helium-neon laser beam which has been collimated and stopped to an aperture of 0.10 inch passes downward through a beam-splitting mirror. A portion of the beam is reflected and the remainder passes through the mirror to the sample cell. The sample cell is tilted slightly so that the portion of the laser light which is reflected off the cell window does not follow the same path as the light which is reflected off the liquid surface. The light reflected off the liquid surface is a converging beam and passes upward through the cell window. A portion of this converging beam is reflected off the beam-splitting mirror and travels horizontally along a calibrated scale. At some point along its path the light reflected off the liquid surface constricts to a minimum cross section and this position, which corresponds to the liquid surface focal length, can be used to determine r_o. The focus may occur anywhere between quite close to the liquid and many meters away, depending on the value of B_1. As shown in Figure 2.2-3, a lens can be used to transfer the focal point further from the liquid surface. Figure 2.2-4 shows how a lens can be used to transfer the focal point closer to the liquid surface. These transfer techniques are useful in bringing the focus to an easily measured position.

Due to the small diameter of the laser beam and the speckle effect induced by the coherent nature of its light, it is sometimes difficult to detect the exact focus of the cell using visual techniques. As a result of these difficulties an electronic focus detector has been built for use with the optical tensiometer. The focus detector consists of a disk covered with parallel opaque and transparent lines. This grating is mounted on a support spider and is rotated by a 400 RPM synchronous motor. The rotating grating is placed in the beam of light reflected from the liquid surface. Behind

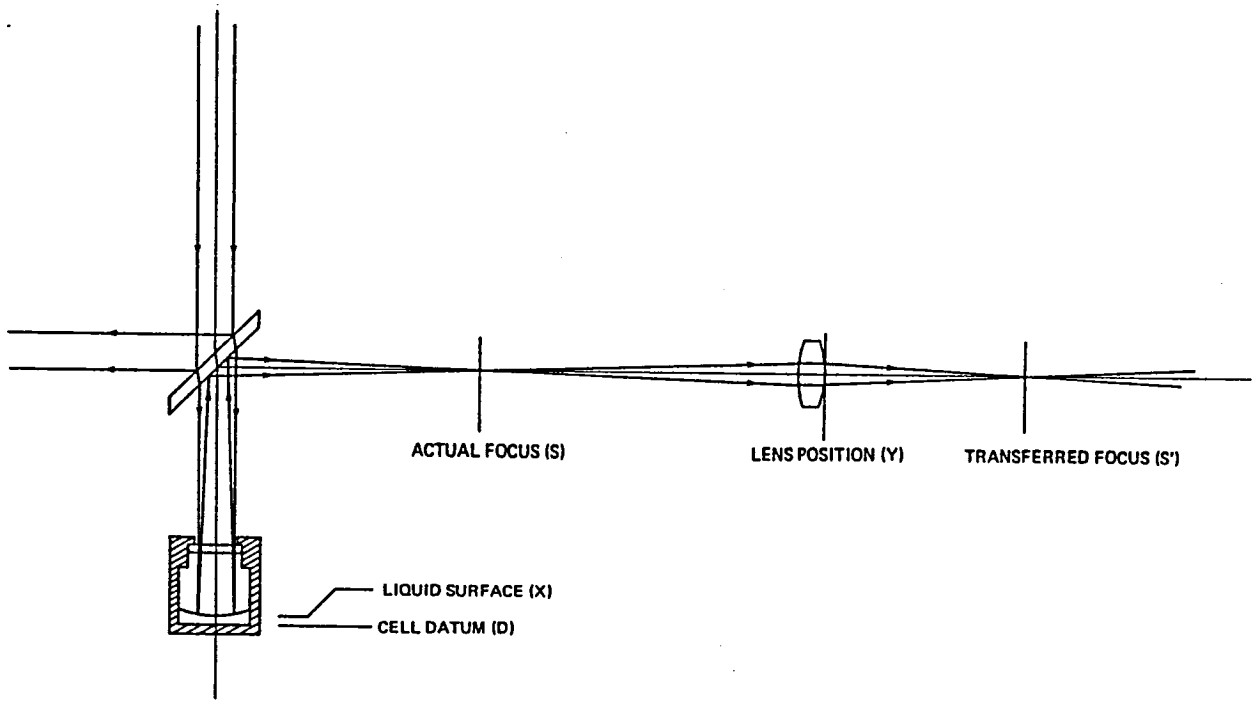

Figure 2.2-3

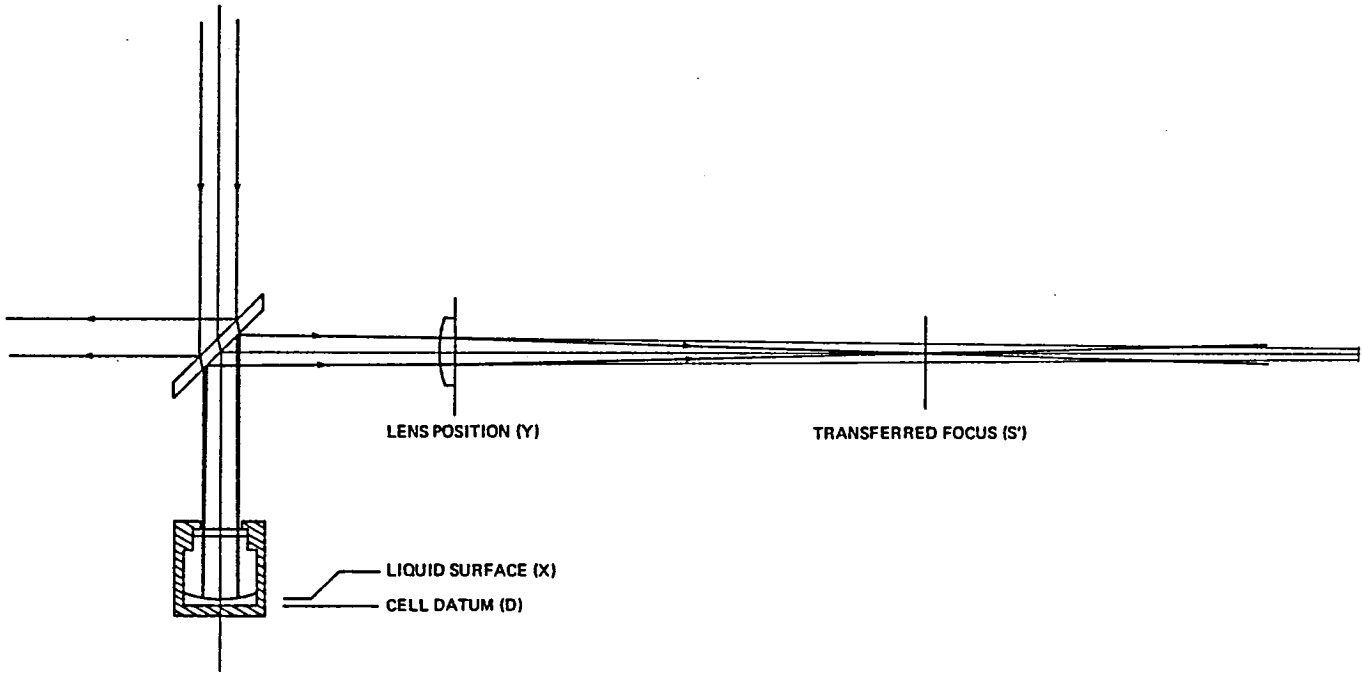

Figure 2.2-4

Schematic Diagrams of the Optical Tensiometer

the grating is a silicon photocell. The output signal of the photocell is a series of pulses the amplitude of which is determined by how closely the focal point of the cell and the plane of rotation of the grating coincide. This signal is amplified and then filtered to remove any low frequency components. The conditioned signal is then rectified and the resulting DC voltage is displayed on a digital readout. A peak in the meter reading versus position of the grating corresponds to the focus of the cell.

2.3 Viscosity Measurement

Selection of a viscosity-measuring technique for heat pipe fluids requires consideration of nominal fluid operating temperatures, operating pressures, and viscosities. For example, viscosity measurements for low vapor pressure fluids are much less difficult than for high vapor pressure working fluids because the problem of fluid containment is minimized. All techniques for viscosity measurement by definition measure fluid drag, and to magnify the drag effect it is common practice to either measure flow rate through a small orifice or capillary, or to measure the drag between two surfaces in close proximity. In either case, the operating temperature range is critical because of possible changes in orifice or surface-to-surface gap size. Commercial viscometers sold by laboratory supply houses are summarized in Table 2.3-1 on the basis of viscometer types, operating temperature range, viscosity range, and accuracy.

Table 2.3-1

OPERATING CHARACTERISTICS OF COMMERCIAL VISCOMETERS

Viscometer Type	Nominal Operating Temperature Range (°C)	Viscosity Range (Centipoise)	Stated Accuracy (%)
Capillary tube/ orifice	0 to 250	0.33 to 10^5	±0.35
Rotating cylinder	--	2.0 to $4(10^5)$	±5.0
Falling Ball	-60 to 150	0.01 to 10^5	±0.5
Viscosity Balance	-60 to 300	0.01 to 10^7	±1.0

The capillary tube/orifice viscometer operates by measuring fluid flow rate through a restriction under a known driving pressure. This type of viscometer is typically used for measuring viscosities of various petroleum oils, and as such the devices are used over the temperature range 0 to 250°C, with restrictions available for the approximate viscosity range 0.33 to 10^5 centipoise. An accuracy of 0.35% is typical.

In the rotating cylinder viscometer, the drag of a fluid on a rotating cylinder within a chamber is measured. This type is again used primarily for petroleum oils and attachments may be purchased to cover the viscosity range 2 to $4(10^5)$ centipoise with an accuracy of ±5%.

Falling ball and viscosity balance viscometers both employ a hollow tube and sphere. Viscosity is determined by measuring the rate at which the sphere moves in the tube bore, propelled either by the action of gravity (falling ball) or by the action of an external load (viscosity balance). The falling ball viscometer has an operating range of 0.01 to 10^5 centipoise at an accuracy of ±0.5%. The temperature range is -60 and 150°C. Viscosity balances may be found that cover the extremely wide range of 0.01 to 10^7 centipoise at a 1% level of accuracy. Their temperature range is -60 to 300°C.

2.3.1 Viscosity Measurement: Selected Approach

Most heat pipe fluids are relatively nonviscous, and an operating range from 0.10 to 10.0 centipoise is desirable. Heat pipe fluids are generally operated at pressures from several mm of mercury to about 10 atmospheres, and a viscometer is needed that could cover this entire range of pressure. The present investigations concern operating temperatures from essentially lab ambient to 350°C, and it is desirable for the viscometer to cover this entire temperature band, if possible. A viscometer requiring a relatively small liquid sample is also desired since many fluids may be available in laboratory quantities only.

On the basis of these viscometer criteria, a falling ball type of device was selected as most appropriate for the measurement of heat pipe working fluid viscosities. The falling ball has a large dynamic range extending down to 0.01 centipoise and an accuracy on the order of 0.5 to 1.0%. However, a viscometer satisfying all criteria was not commercially available, and a unit was built that is specifically designed for heat pipe fluid viscosity measurements.

Figure 2.3-1 is a schematic of the system designed for this project. A glass capillary tube of about 0.8 mm I.D. is used as the liquid sample holder, and a sapphire sphere is used as the falling ball. Borosilicate capillary tubes of adequate precision are readily available; nominal bores that do not change by more than ±0.00254 mm over a few centimeters of length are standard items, and sapphire microspheres are available that are accurate to about $\pm 2.5(10^{-4})$ mm sphericity and diameter.

To accurately measure viscosity, a method of precisely determining the rate of fall of the ball also had to be devised. For this program, an optoelectronic timing approach was successfully used. The refractive index of sapphire is on the order of 1.75, while borosilicate glass and most working fluids have refractive indexes in the range 1.45 to 1.55. Therefore, if a small beam of light impinges on the capillary bore, when the sapphire ball passes there will be a substantial change in transmitted light through the tube central region. This change can be easily detected by a phototransistor focused onto the capillary bore as in Figure 2.3-1, and can be used to start and stop a quartz crystal timer. The essential elements of a falling ball viscometer are therefore all present: a precision bore tube, falling ball, and timer.

2.3.2 Theory

The drag on the sphere as it falls down the tube can be expressed as:

$$\text{Drag} = \frac{\pi d^2}{4} \frac{1}{2} \rho_\ell \, u_t^{\,2} \, f\left(\frac{d}{D}, \, \text{Re}_d, \, \theta\right) \qquad 2.3\text{-}1$$

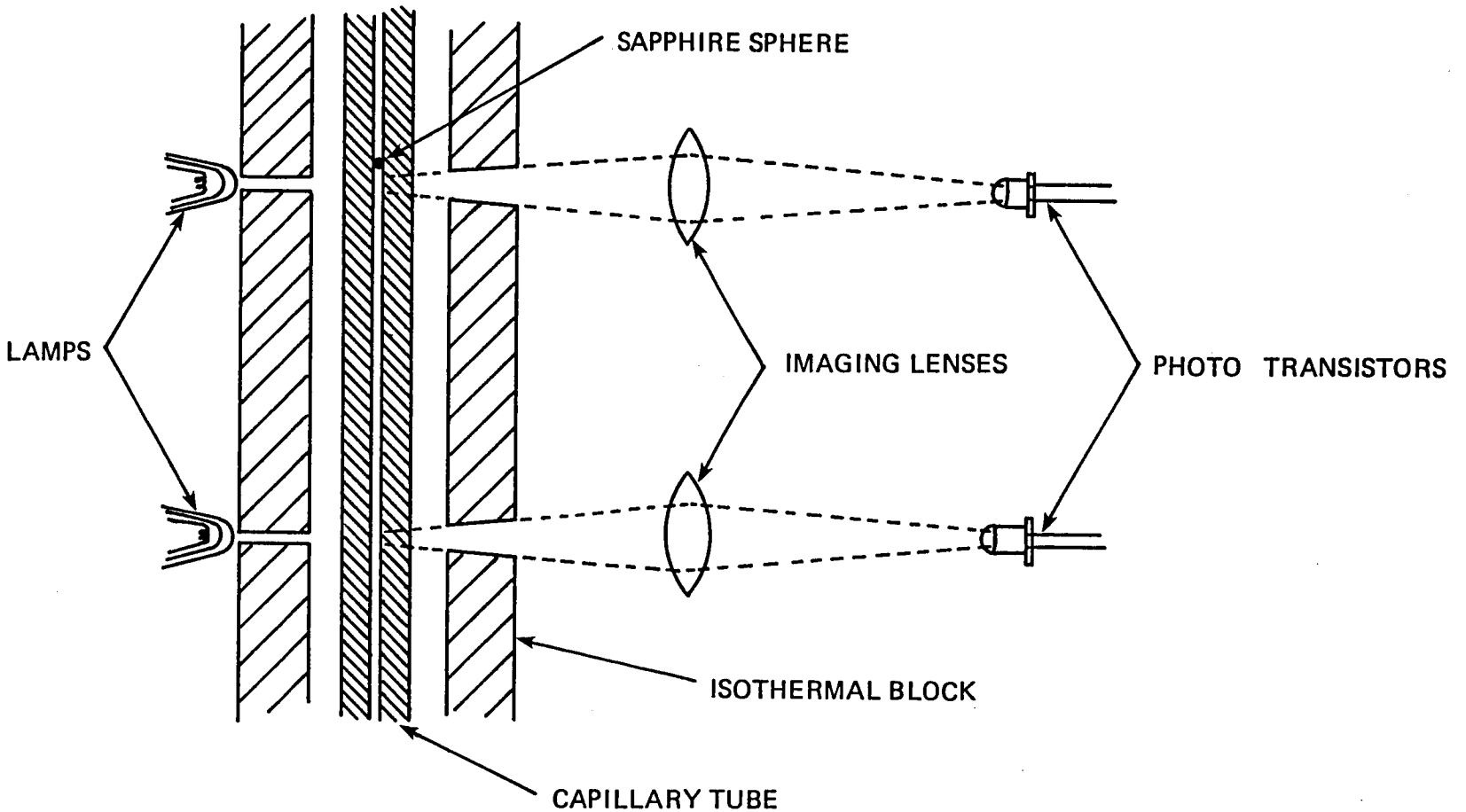

Figure 2.3-1. Schematic of the Falling Ball Viscometer.

where: d = diameter of sphere

D = diameter of capillary

ρ_ℓ = liquid density

u_t = terminal velocity of sphere

f = friction factor based on the diameter ratio. The Reynolds number Re_d is based on the sphere diameter, and θ is the tilt angle.

The force on the sphere in the direction of travel due to gravity is given by:

$$\text{Force} = \frac{\pi d^3}{6} \rho_s \, g \, \sin(\theta) \qquad 2.3\text{-}2$$

where: ρ_s = sphere density

g = acceleration of gravity

θ = angle from horizontal

Equations 2.3-1 and 2.3-2 can be set equal to each other and solved for $f\left(\frac{d}{D}, Re_d, \theta\right)$.

$$f\left(\frac{d}{D}, Re_d, \theta\right) = \frac{4}{3} \frac{\rho_s}{\rho_\ell} \frac{d \, g \, \sin(\theta)}{u_t^2} \qquad 2.3\text{-}3$$

Thus by measuring u_t with the falling ball viscometer and knowing g, θ, ρ_s, and ρ_ℓ, it is possible to compute the value of f for the conditions of the experiment. If the value of f as a function of d/D, Re_d, and θ is known, then the viscosity u can be calculated via the Reynolds number.

In the limit of an infinitely large vertical tube, the Reynolds number-friction factor relations for terminal velocity conditions in an incompressible fluid are

$$Re = 24/f \qquad (Re \leq 0.1 \text{ to } 2.0)$$

$$Re \cong 129.4/f^{5/3} \qquad (2.0 \leq Re \leq 1000)$$

For d/D up to about 0.1, a more accurate representation for creeping flow is given by inclusion of the Ladenburg-Faxen correction,[9]

$$Re = \frac{24}{f}\left(1 + 2.1\,\frac{d}{D}\right) \qquad (Re \leq 0.1 \text{ to } 2.0) \qquad 2.3\text{-}4$$

For values of d/D approaching 1.0, some investigators have assumed that the area of closest-approach between the sphere and cylinder can be approximated by two flat plates, and the Reynolds number given by[10]

$$Re = \frac{40}{f\left(1 - \frac{d}{D}\right)^{2.5}} \qquad (Re \leq 0.1 \text{ to } 2.0) \qquad 2.3\text{-}5$$

There is unfortunately no completely tested theory for the entire range of d/D, and very little study at all has been directed towards tilted systems. However, if all experiments are done with the same size spheres and capillaries, and at the same tilt, it is not necessary to know the functional dependence of f on the diameter ratio d/D, or on θ. Thus f is effectively only a function of the Reynolds numbers and conversely the Reynolds number is a function only f. For a 60° tilt angle, and d/D = 0.861 the functional dependence of f on the Reynolds number has been experimentally determined to be:

$$f\left(Re_d\right) = \exp\left(8.49387 - 1.06466 \ln Re_d + 0.0260677\left[\ln\left(Re_d\right)\right]^2\right) \qquad 2.3\text{-}6$$

$$100 \leq f \leq 3200 \qquad 1.3 \leq Re_d \leq 50$$

This equation can be iteratively solved for Re_d in the following manner:

$$\ln\left(Re_d\right)_{n+1} = \frac{8.49387 - \ln(f) + 0.0260677\left[\ln\left(Re_d\right)\right]^2_n}{1.06466} \qquad 2.3\text{-}7$$

Thus measuring u_t with the viscometer allows one to compute f which can than be used to determine Re_d. Finally given Re_d the liquid viscosity is given by:

$$u = \frac{\rho_\ell \, u_t \, d}{Re_d} \qquad 2.3\text{-}8$$

2.4 Physical Property Measurements

2.4.1 Surface Tension

Surface tension data were experimentally obtained for napthalene and diphenyl using the optical tensiometer. Data were taken from the melting points to approximately 275°C. In addition the surface tension of benzene was measured and compared with values presented in the Heat Pipe Design Handbook.[11]

A detailed description of the optical tensiometer can be found in Section 2.2. Briefly, the optical tensiometer consists of a device for measuring the radius of curvature of the liquid meniscus formed within a sealed cylindrical sample cell. The ratio of the cell radius to the radius of curvature of the liquid surface is then related to the Bond number of the liquid based on the cell radius. If the liquid and vapor densities are known or can be estimated the surface tension of the liquid within the cell can be computed.

Tables 2.4-1 through 2.4-3 contain the results of the measurements taken on these fluids. Values of the meniscus radius of curvature, R_o, were measured

using the optical tensiometer. The cell radius, R_1, was known to be 1.02 cm. The Bond number based on the cell radius, B_1, was calculated using the following relation which is a least squares fit to the numerical solution of the governing differential equations.

$$\ell n(B_1) = -0.854857 + 1.64627\ \ell n\left(\frac{R_1}{R_o}\right) + 0.27662\left[\ell n\left(\frac{R_1}{R_o}\right)\right]^2 +$$

$$0.0500133\left[\ell n\left(\frac{R_1}{R_o}\right)\right]^3 + 0.00267328\left[\ell n\left(\frac{R_1}{R_o}\right)\right]^4 \qquad 2.4\text{-}1$$

when $0.003 \leq \left(\frac{R_1}{R_o}\right) \leq 0.2$.

Table 2.4-1

RESULTS OF MEASUREMENTS USING BENZENE

T, °C	R_1/R_o	B_1	$\rho_\ell - \rho_v$	γ_{NASA}	γ_{EXPTL}	γ_{B+B}
31.3	0.05136	0.02948	0.867	27.54	26.1	26.6
46.2	0.04766	0.02852	0.851	25.68	24.8	24.8
65.6	0.03868	0.02607	0.831	23.31	22.1	22.4
78.0	0.03469	0.02494	0.817	21.81	20.8	20.9
89.8	0.03148	0.02399	0.803	20.38	19.7	19.4
102.7	0.02707	0.02263	0.786	18.82	18.2	17.9
117.3	0.02134	0.02073	0.767	17.06	16.2	16.2
133.4	0.01611	0.01878	0.745	15.12	14.3	14.4
149.4	0.01156	0.01682	0.728	13.19	12.5	12.6
165.8	0.00694	0.01436	0.705	11.22	10.3	10.8
180.7	0.00386	0.01220	0.679	9.45	8.4	9.2

Table 2.4-2

RESULTS OF MEASUREMENTS USING NAPTHALENE

T, °C	R_1/R_o	B_1	$\rho_\ell - \rho_v$	γ_{EXPTL}	γ_{B+B}
94.9	0.06662	0.03334	0.967	32.90	32.01
103.1	0.06499	0.03294	0.961	32.31	31.17
117.6	0.06499	0.03294	0.949	31.91	29.70
138.6	0.04700	0.02834	0.932	26.96	27.58
154.3	0.04293	0.02725	0.919	25.56	26.01
171.8	0.03728	0.02568	0.905	23.72	24.29
172.2	0.03639	0.02543	0.905	23.49	24.25
184.5	0.03304	0.02445	0.894	22.31	23.05
197.7	0.02829	0.2302	0.883	20.75	21.78
214.6	0.02329	0.02140	0.867	18.94	20.17
230.3	0.01930	0.02000	0.852	17.39	18.70
244.3	0.01740	0.01929	0.839	16.52	17.40
245.6	0.01523	0.01843	0.837	15.74	17.28
262.2	0.01248	0.01725	0.820	14.44	15.77
273.5	0.01103	0.01657	0.808	13.66	14.75

Table 2.4-3

RESULTS OF MEASUREMENTS USING DIPHENYL

T, °C	R_1/R_o	B_1	$\rho_\ell-\rho_v$	γ_{EXPTL}	γ_{B+B}
77.9	0.08606	0.03807	0.987	38.35	37.13
110.3	0.07793	0.03611	0.963	35.49	33.80
174.9	0.04364	0.02744	0.915	25.62	27.34
212.8	0.02943	0.02337	0.885	21.11	23.67
256.2	0.01784	0.01945	0.848	16.83	19.60
277.6	0.01355	0.01772	0.828	14.97	17.64

$$B_1 = \frac{\gamma}{\left(\rho_\ell-\rho_v\right) g\ R_1^2}$$

where: γ = surface tension (dynes/cm)

ρ_ℓ = liquid density (g/cm^3)

ρ_v = vapor density (g/cm^3)

g = acceleration of gravity (cm/sec^2)

R_1 = cell radius (cm)

Liquid densities were estimated using the technique of Gunn and Yamada.[12] This technique requires knowledge of the critical temperature, T_c, critical pressure, P_c, acentric factor, ω, and a known value of the density at some reference temperature. Vapor densities were calculated using the Redlich-Kwong equation of state.[13] Again, knowledge of the critical properties was required. In addition, knowledge of the vapor pressure was needed. When the necessary coefficients were available the Harlacher vapor pressure equation was used.[14] In other cases, vapor pressure was calculated using Antoine's vapor pressure equation.[15] The values of $\rho_\ell-\rho_v$ used are presented in each table.

Table 2.4-1 presents the value of surface tension obtained from the Heat Pipe Design Handbook, γ_{NASA}, as well as the experimentally determined value, γ_{EXPTL}, obtained with the optical tensiometer. In addition, each table presents a predicted value of surface tension, γ_{B+B}, based on the corresponding states correlation of Brock and Bird.[16]

The benzene references and measured data generally agree to within ±5%. Operating experience indicates that the system's accuracy can be further improved by optimizing the grating on the focus detector and optimizing the cell and heater block designs to minimize thermal gradients.

2.4.2 Viscosity

Two fluids were examined using the falling ball viscometer. One fluid was benzene, a relatively common fluid used to verify the accuracy of the instrument. The other liquid examined was 1-fluoronapthalene. 1-fluoronapthalene is potentially a very suitable fluid for use in moderately high temperature heat pipes. This is a result of its resistance to thermal decomposition and the wide range between its normal boiling and freezing points.

Table 2.4-4 presents the experimentally measured values of viscosity as well as as comparison values. In the case of benzene the comparison values were obtained from the Heat Pipe Design Handbook.[11] The experimentally measured values of viscosity for benzene were typically within five percent of the handbook values. Comparison values of viscosity for 1-fluoronapthalene were calculated using the Orrick and Eber correlation[17] which uses a group contribution technique based on the molecular structure of the compound. The average error for this method when applied to organic liquids has been estimated to be approximately 15 percent. The experimentally measured values of viscosity for 1-fluoronapthalene were typically within 17 percent of the calculated values.

Table 2.4-4

RESULTS OF VISCOSITY MEASUREMENTS FOR 1-FLUORONAPTHALENE AND BENZENE

1-Fluoronapthalene

T(°C)	$1/T(K^{-1})$	u_{exp}(cP)	u_{calc}(cP)
22.5	3.38-03	2.12	2.49
37.6	3.22-03	1.66	1.96
60.8	2.99-03	1.21	1.42
85.0	2.79-03	0.897	1.06
108.1	2.62-03	0.698	0.827
133.2	2.46-03	0.543	0.653
172.2	2.25-03	0.385	0.478
212.1	2.06-03	0.291	0.365

Benzene

T(°C)	$1/T(K^{-1})$	u_{exp}(cP)	u_{NASA}(cP)
7.8	3.56-03	0.744	0.775
16.4	3.45-03	0.657	0.680
31.5	3.28-03	0.547	0.547
37.8	3.22-03	0.534	0.503
79.9	2.83-03	0.292	0.311
106.4	2.63-03	0.228	0.243
128.1	2.49-03	0.192	0.201
146.4	2.38-03	0.168	0.171

As a further check of this technique of measuring viscosity, experimental data are plotted on a log scale versus the reciprocal of the absolute temperature in Figure 2.4-1. When plotted this way the data should result in a straight line. For convenience the data are plotted versus temperature in degrees Celsius in Figure 2.4-2 along with the comparison values from Table 2.4-4.

2.5 Demonstration Heat Pipes

Two 6061 alloy aluminum heat pipes of 0.5-inch-square cross section have been charged with the working fluids napthalene (SN/74) and titanium tetrachloride (SN/75). The heat pipes incorporate a 0.43 cm I.D. core which has a circumferential 100-inch V-groove thread along the entire wall. The pipes also use a multiple-tube screened artery to assist in axial liquid transport. The artery consists of nineteen 400-mesh stainless screen tubes of approximately 0.032 inch O.D. clustered into a bundle with a nominal diameter of 0.180 inch. The centrally located tube bundles communicate to the wall via two diametrically opposed 200-mesh stainless screen stems. With anhydrous ammonia working fluid, the heat pipes will typically show a capacity in excess of 3000 watt-inches.

After charging, the heat pipes were operated in reflux for a period of 15 hours at 230°C and 150°C respectively for SN/74 and SN/75. At the end of that time, the heat pipes were vented at a pressure slightly in excess of atmospheric until no cold leg was observed at the extreme condenser end. The heat pipe valves were then closed, capped, and packed for shipment to Lewis Research Center.

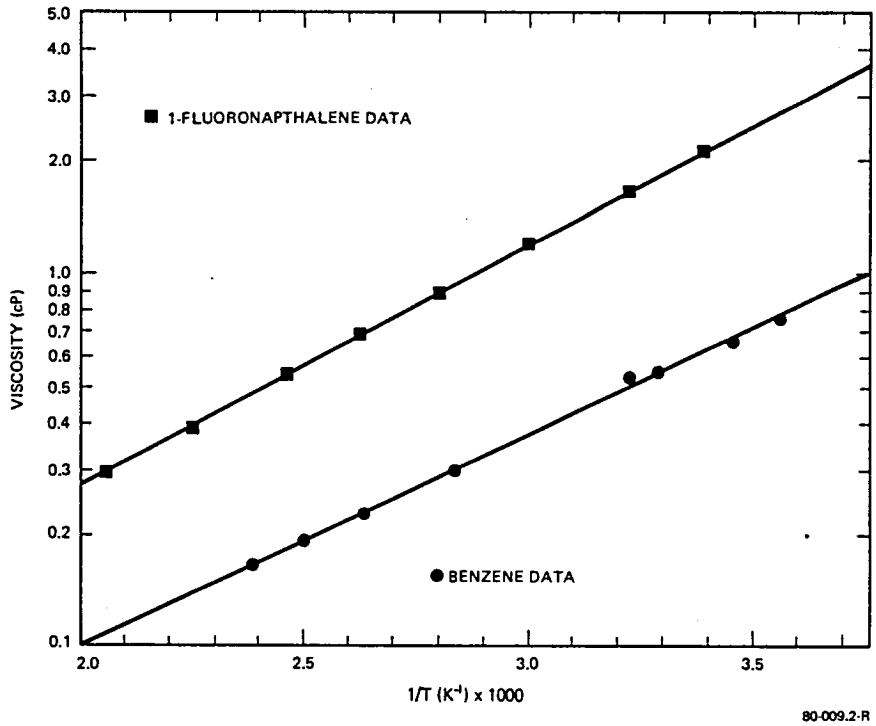

Figure 2.4-1. Log Viscosity Versus 1/T for 1-Fluoronapthalene and Benzene.

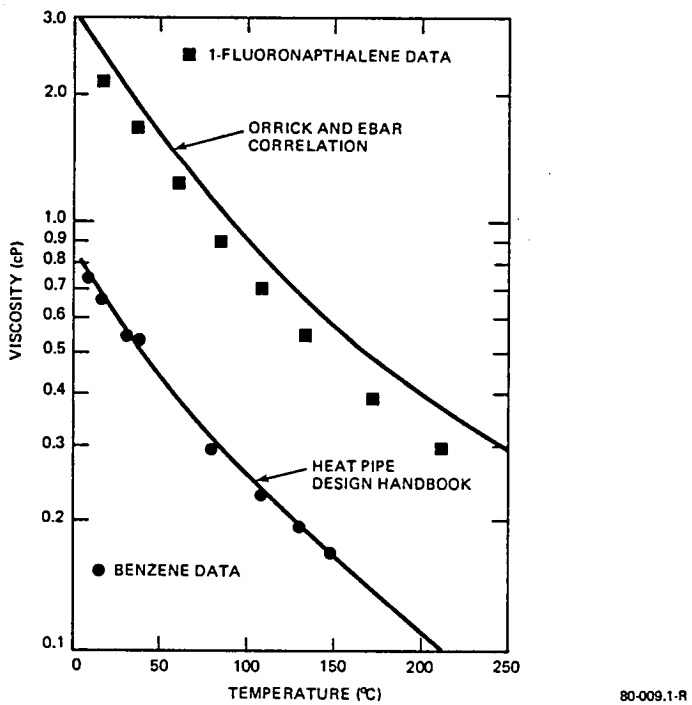

Figure 2.4-2. Viscosity Versus Temperature for Fluids Tested.

3.0 REFERENCES

1. Two Phase Working Fluids for the Temperature Range 50° to 350°C, Contract NAS3-20222, final report CR-135255, June 1977.

2. Olin Chemicals, Handbook of Aromatic Fluorine Compounds, Olin Corp., 120 Long Ridge Road, Stamford, CT 06904.

3. Brochure Halowax® Chlorinated Napthalene Oils and Waxlike Solids, Koppers Company, Inc., 612 Chatham Center, Pittsburgh, PA.

4. Personal communication with R. W. Maxwell, Jr., Group Leader, Industrial Chemicals, Koppers Company, Inc., Organic Materials Div., 440 College Park Drive, Monroeville, PA 15146.

5. Sample provided by R. E. Moore, Suntech, Inc., P.O. Box 1135, Marcus Hook, PA 19061.

6. A. W. Adamson, Physical Chemistry of Surfaces, Interscience Publishers, New York, NY, 1967.

7. S. Sugden, J. Chem. Soc., 119, p. 1483-1492, 1921.

8. Lord Rayleigh, Proc. Roy. Soc., 1915, [A], 92, p. 184.

9. R. Bird, W. Stewart, E. Lightfoot, Transport Phenomena, John Wiley and Sons, New York, NY, 1966.

10. S. Uno and R. Kintner, AICHE J., 2, p 420, 1956.

11. Heat Pipe Design Handbook, prepared for NASA by B&K Engineering, Inc., Towson, MD, 1979.

12. The Properties of Gases and Liquids, Third Edition, R. C. Reid, J. M. Prausnitz, T. K. Sherwood, McGraw-Hill Book Company, New York, NY, p. 60-61, 1977.

13. Ibid, p. 37-38.

14. Ibid, p. 189.

15. Ibid, p. 184-185.

16. Ibid, p. 605-608.

17. Ibid, p. 439-441.

FINAL REPORT DISTRIBUTION LIST

Contract NAS3-21202

NASA CR-159847

One copy for each except as noted.

NASA Lewis Research Center
21000 Brookpark Road
Cleveland, OH 44135
Attn: H. Mark (M.S. 77-4)
I. T. Myers (M.S. 77-4)
L. Gedeon (M.S. 77-4) (4 copies)
Propulsion & Power Section (M.S. 500-306)
Report Control Office (M.S. 5-5)
Library (M.S. 60-3) (2 copies)
Technical Utilization Office (M.S. 7-3)
Patent Counsel (M.S. 500-318)

NASA Scientific and Technical Information Facility (9 copies)
Attn: Accessioning Department
P. O. Box 8757
Baltimore/Washington International Airport, MD 21240

E. E. Bailey
AFAPL/DO
Wright-Patterson AFB, OH 45433

NASA Headquarters
Attn: RWM/B. Achhammer
Washington, DC 20546

NASA Goddard Space Flight Center
Attn: 732.1/S. Ollendorf
Greenbelt, MD 20771

NASA Langley Research Center
Attn: Robert Greene, M.S. 434
Langley Station
Hampton, VA 23365

NASA Johnson Space Center
Attn: ES3/E. Chimenti
Houston, TX 77058

NASA Johnson Space Center
Attn: EC2/W. Guy
Houston, TX 77058

NASA Marshall Space Flight Center
Attn: G. Robinson, S&E, ASTN-PTC
Marshall Space Flight Center, AL 35812

NASA Ames Research Center
Attn: Craig R. McCreight, M.S. 244-7
Moffett Field, CA 94035

FINAL REPORT DISTRIBUTION LIST

Mr. J. P. Alario
Grumman Aerospace Corporation
Bethpage, NY 11714

Dave Almgren
Arthur D. Little, Inc.
Cambridge, MA 02140

Mr. S. J. Babjak
AFML MBE
Wright-Patterson AFB, OH 45433

Mr. Algerd Basiulis
Hughes Aircraft Company
Electron Dynamics Division
3100 West Lomita Boulevard
Torrance, CA 90509

Dr. Walter B. Bienert
Dynatherm Corporation
One Industry Lane
Cockeysville, MD 21030

Mr. L. E. Blomstrom
General Electric
Space Systems Organization
Valley Forge Space Center
P. O. Box 8555
Philadelphia, PA 19181

Mr. P. J. Brennan
B&K Engineering, Inc.
One Investment Place
Suite 825
Towson, MD 21204

Mr. Andy T. Calimbas
Engineering Specialist
General Electric
Space & Re-entry Systems Div.
3875 Fabian WAy
Palo Alto, CA 94303

Dr. A. Cenkner
Perkin-Elmer Corporation
100 Wooster Heights Road
Danbury, CT 06810

Bob Chimenti
ESSO Research & Engineering Co.
P. O. Box 8
Linden, NJ 07036

Prof. G. T. Colwell
Dept. of Mechanical Engineering
Georgia Institute of Technology
Atlanta, GA 30332

Dr. Creighton Depew
Department of Mechanical Engineering
University of Washington
Seattle, WA 98105

Dr. J. E. Deverall
Los Alamos Scientific Lab.
University of California
Los Alamos, NM 87544

Mr. G. Yale Eastman
Thermacore, Inc.
Box 135
Leola, PA 17540

Mr. R. A. Farran
The Aerospace Corporation
2350 East El Segundo Boulevard
El Segundo, CA 90245

Prof. K. T. Feldman
Department of Mechanical Engineering
University of New Mexico
Albuquerque, NM 87106

Prof. J. K. Ferrell
Department of Chemical Engineering
North Carolina State University
Raleigh, NC 27607

Mr. W. Harwell
Grumman Aerospace Corporation
P. O. Box 31
Bethpage, NY 11714

Mr. William L. Haskin
Air Force Flight Dynamics Lab.
Code FEE
Wright-Patterson AFB, OH 45433

Professor Tom Jones
Colorado State University
Dept. of Electrical Engineering
Fort Collins, CO 80521

Dr. Y. Kamotani
Dept. of Mechanical & Aerospace
Engineering
Case Western Reserve University
Cleveland, OH 44106

FINAL REPORT DISTRIBUTION LIST

Prof. Matthew D. Kelleher
Naval Postgraduate School
Dept. of Mechanical Engineering
Monterey, CA 93940

Mr. J. E. Kemme
Q-25, M.S. 576
Los Alamos Scientific Laboratory
P. O. Box 1663
Los Alamos, NM 87544

Mr. James H. Kidd
Thermophysics Section
Martin Marietta Corporation
P. O. Box 179
Denver, CO 80201

Dr. Robert L. Kosson
Grumman Aerospace Corporation
Bethpage, NY 11714

Mr. David Antoniuk
TRW Defense and Space Systems Group
One Space Park
Redondo Beach, CA 90278

Prof. R. I. Loehrke
Dept. of Mechanical Engineering
Colorado State University
Fort Collins, CO 80523

Mr. R. Masek
McDonnell Douglas Astronautics Co./East
P. O. Box 516
St. Louis, MO 63166

Dr. Harris B. McKee
McDonnell Douglas Astronautics Co./East
P. O. Box 516
St. Louis, MO 63166

Mr. R. K. McMerdie
Martin Marietta
P. O. Box 179
Mail N. S-8940
Denver, CO 80201

Prof. Arun S. Mujumdar
Dept. of Chemical Engineering
McGill University
P. O. Box 6070, Station A
Montreal, Quebec
CANADA H3C 3G1

Dr. Dave Murray
LMSC Bldg. 205, Dept. 5221
3251 Hanover Street
Palo Alto, CA 94304

Mrs. Peggy Myers, Librarian
Anchor Hocking Corporation
General Development Laboratory
West Fair Avenue
Lancaster, OH 43130

Mr. R. Pessolano
Isothermics, Inc.
P. O. Box 86
Augusta, NJ 07822

Jet Propulsion Laboratory
Attn: W. Petrick, M.S. 157-102
4800 Oak Grove Drive
Pasadena, CA 91103

John Pogson
Boeing Company
Aerospace Group
P. O. Box 3999
Seattle, WA 98124

Dr. Robert Richter
Xerox Corporation
Electro-Optical Systems
300 N. Halstead Street
Pasadena, CA 91107

J. S. Schaming
Dept. 242-027 GB30
Autonetics
3370 Mira Loma
Anaheim, CA 92806

Bruce Schelden
Martin Marietta Co., M.S. C-3740
P. O. Box 179
Denver, CO 80201

Maj. P. Sivgals
SAMSO/Code DYL
P. O. Box 92960
Department of the Air Force
Headquarters, L. A. Air Force Station
Worldway Postal Center
Los Angeles, CA 90009

FINAL REPORT DISTRIBUTION LIST

Dr. Y. S. Tang
Westinghouse Electric Corp.
P. O. Box 10864
Pittsburgh, PA 15236

Mr. G. M. Grover
Q-Dot Corporation
151 Regal Row, Suite 120
Dallas, TX 75247

Prof. Chang-Lin Tien, Chairman
Dept. of Mechanical Engineering
University of California
Berkeley, CA 94720

Prof. P. C. Wagner, Jr.
Dept. of Chemical & Environmental
Engineering
Rensselaer Polytechnic Institute
Troy, NY 12181

Mr. J. P. Wright
Rockwell International
Space Division SL32
12213 Lakewood Boulevard
Downey, CA 90241

Dr. H. Yanowitz
Perkin-Elmer Corporation
100 Wooster Heights Road
Danbury, CT 06810